tadata, citation and similar papers at core.ac.uk

Available online at www.sciencedirect.com

SCIENCE DIRECT®

ELSEVIER

Ecological Modelling 168 (2003) 109–143

ECOLOGICAL MODELLING

www.elsevier.com/locate/ecolmodel

Mathematical modelling to assess the carrying capacity for multi-species culture within coastal waters

P. Duarte [a,*], R. Meneses [a], A.J.S. Hawkins [b], M. Zhu [c], J. Fang [d], J. Grant [e]

[a] *IMAR—Departamento de Ciências e Engenharia do Ambiente, Universidade Nova de Lisboa, 2825-114 Monte de Caparica, Portugal*
[b] *Plymouth Marine Laboratory, Prospect Place, The Hoe, Plymouth PL1 3DH, UK*
[c] *State Oceanic Administration, First Institute of Oceanography, Xianxialing Road, 266061 Qingdao, PR China*
[d] *Yellow Sea Fisheries Research Institute, 106 Nanjing Road, 266071 Qingdao, PR China*
[e] *Department of Oceanography, Dalhouise University, Halifax, NS, Canada B3H 4J1*

Received 7 May 2002; received in revised form 21 March 2003; accepted 20 May 2003

Abstract

In the context of aquaculture, carrying capacity is generally understood as the standing stock of a particular species at which production is maximised without negatively affecting growth rates. The estimation of carrying capacity for aquaculture is a complex issue. That complexity stems from the many interactions between and among cultivated and non-cultivated species, as well as between those species and their physical and chemical environments. Mathematical models may help to resolve these interactions, by analysing them in a dynamic manner. Previous carrying capacity models have considered the biogeochemical processes that influence growth of cultivated species in great detail. However, physical processes tend to have been addressed very simplistically. Further, most modelling has been for monocultures, despite the increasing importance of multi-species (=polyculture) systems.

We present here a two-dimensional coupled physical–biogeochemical model implemented for Sungo Bay, Shandong Province, People's Republic of China. Sungo Bay is used for extensive polyculture, where bivalve shellfish and kelp are the most important cultivated species. Data collected over 13 years (1983–2000) was available for modelling. Our main objectives were to implement the model, achieving reasonable calibration and validation with independent data sets, for use in estimating the environmental carrying capacity for polyculture of scallops and oysters.

Findings indicate that the model successfully reproduces some of the main features of the simulated system. Although requiring some further work to improve predictive capability in parts, predictions clearly indicate that Sungo Bay is being exploited close to the environmental carrying capacity for suspension-feeding shellfish. Comparison of different culture scenarios also indicates that any significant increase in yield will depend largely on a more optimal spatial distribution of the different cultivated species.
© 2003 Elsevier B.V. All rights reserved.

Keywords: Ecological modelling; Carrying capacity; Multi-species culture

1. Introduction

Estuaries and semi-enclosed bays are intensively used for aquaculture in many countries. Suspension-feeding bivalves are among the most cultivated organisms in these ecosystems. This is a "passive" type of culture, where the animals feed

* Corresponding author. Present address: CEMAS—University Fernando Pessoa, Praça 9 de Abril 349, 4249-004 Porto, Portugal. Tel.: +351-22-507-1300; fax: +351-22-550-8269.
E-mail address: pduarte@ufp.pt (P. Duarte).

0304-3800/$ – see front matter © 2003 Elsevier B.V. All rights reserved.
doi:10.1016/S0304-3800(03)00205-9

on natural suspended matter, their metabolites being dispersed by currents and waves.

The concept of environmental carrying capacity is not only important for species cultivation but also for other concerns such as water quality and tourism. With respect to bivalve culture, carrying capacity has been defined as the maximum standing stock that may be kept within a particular ecosystem to maximise production without negatively affecting growth rate (Carver and Mallet, 1990). Alternatively, and more recently, carrying capacity has been described as the standing stock at which the annual production of the marketable cohort is maximised (Bacher et al., 1998). There are several other definitions of carrying capacity for aquaculture in the literature. However, these are generally concerned with the culture of a single target species, despite a growing tendency in Eastern Countries for "ecological aquaculture" based on multi-species culture, where producers and consumers are grown together to facilitate nutrient recycling. Here, the objective is not only to maximise production, but also to optimise species combinations and distributions in such a way as to reduce the environmental impacts of aquaculture. The growing appreciation that ecosystems have multiple functions, with a need for integrated management, means that ecologists are increasingly challenged to model the many interactions between and among species, including with their environment, on a large scale. A general definition of carrying capacity at the ecosystem level could be "the level to which a process or variable may be changed within a particular ecosystem, without driving the structure and function of the ecosystem over certain acceptable limits". The definition of "acceptable limits" is very difficult. However, once established in terms of water quality and other parameters, it should be possible to manage different ecosystem uses in a sustainable manner.

There are several examples where carrying capacities for bivalve cultivation have been exceeded by non-sustainable practices. These include the bay of Marénnes-Óleron (France), where oyster (*Crassostrea gigas*) growth has reduced significantly with increased stock densities over the years (Raillard and Ménesguen, 1994). Similarly, mussel (*Mytilus edulis*) growth in the Oosterschelde estuary (The Netherlands) has been compromised by increased standing stocks (Smaal et al., 2001).

Carrying capacities for the culture of suspension-feeding bivalves are primarily limited by rates with which available food is renewed, which is a function of phytoplankton production and water residence time (Dame and Prins, 1998). It is also important to consider the impact of bivalve cultivation itself on water quality, sediment composition and ecosystem functioning. By recycling nitrogen, bivalves may stimulate primary productivity (Smaal et al., 2001). For the same reasons, in line with the concept of ecological aquaculture, bivalves may be successfully cultured alongside kelp, when nutrients excreted and egested by the bivalves may be absorbed by macroalgae and recycled into valuable biomass (Fang et al., 1996). The dynamics of multi-species culture is complex, with many potential positive and negative feedbacks between the cultivated and the non-cultivated species. These feedbacks must be considered when the goal is to optimise production and minimise ecological impacts. For example, macroalgae may compete with phytoplankton for nutrients, and any reduction in phytoplankton biomass may have a negative impact on bivalve growth. In addition, aquaculture structures like rafts and ropes impose drag, thereby reducing current flow and the renewal both of suspended particles for bivalves and of nutrients for kelp (Grant and Bacher, 2001).

To manage such a complex system, these interrelations must all be taken into account. Further, the only way to integrate these interactions is by means of mathematical modelling. Given that different species are distributed in different areas according to their environmental requirements or other criteria, it is important that the models are spatially resolved. Typically, spatially resolved ecological models simulate hydrodynamic transport in a very simple way, considering residual flows and tidally averaged situations. These are known as box models (e.g. Bacher, 1989; Raillard and Ménesguen, 1994; Ferreira et al., 1998). For a description of the general structure of an ecosystem box model with bivalve suspension feeders see Herman (1993) and Dowd (1997). The upscaling of physical transport from hydrodynamic models of high spatial and temporal resolution to biogeochemical models of coarser resolution, as described in Jørgensen and Bendoricchio (2001), has been used by several authors for bivalve carrying capacity modelling (e.g. Bacher, 1989; Raillard and Ménesguen, 1994).

Until recently, relatively little modelling work has been done on the interface between hydrodynamics and biogeochemistry using fully coupled models in marine ecosystems (Dike, 2001). Perhaps one of the most complex ecological models so far developed for a coastal ecosystem was that of the Ems estuary (Baretta and Ruardij, 1988). In spite of the degree of biogeochemical detail present in this model, the physical environment is described in a relatively simple way, using residual flows and diffusion coefficients to parameterise transport.

Although useful in many different ways, box models generally fail to reproduce some important dynamic processes that may affect ecosystem functioning. Among others, these include tidal height variability and its influence on underwater light intensity, as well as current speed dynamics and its influence on sediment resuspension processes, on water turbidity and on water renewal at small spatial scales. The solution to these problems is to have fully coupled physical–biogeochemical models that simulate hydrodynamic transport phenomena including chemical and biological processes within a common framework.

From a practical standpoint, it is very difficult if at all possible to optimise multi-species culture through trial and error. Instead, fully coupled physical–biogeochemical models will enable the comparative assessment of different aquaculture scenarios. Model outputs may then be used to design field trials that may in turn feedback to the models. Iterative application of modelling, field trials and experiments will help to develop understanding of the studied ecosystems, facilitating a more sustainable culture practice.

Main objectives of the work described here were to:

(1) develop a two-dimensional coupled physical–biogeochemical mathematical model for Sungo Bay, Shandong Province, People's Republic of China (Fig. 1) to simulate the aquaculture of

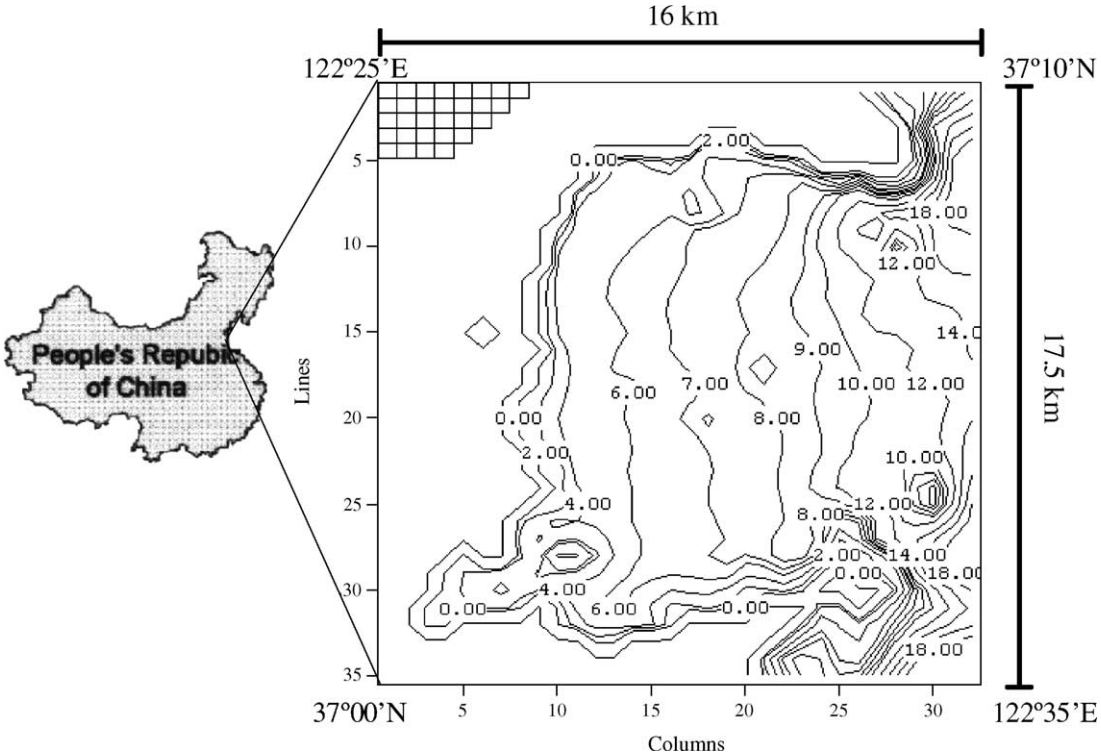

Fig. 1. The location of Sungo Bay, including model domain and bathymetry (m). Also shown, is a part of the model grid (upper left corner), with spatial resolution of 500 m.

suspension-feeding bivalves and kelps, including their interactions with the ecosystem;
(2) calibrate and validate the model with separate data sets;
(3) use the model to assess how current culture practice compares with environmental carrying capacity of the bay;
(4) use the model to analyse the consequences of several possible culture practices for bivalve production in Sungo Bay; and
(5) assess whether our estimates of carrying capacity depend on the degree of spatial detail with which the system is analysed.

2. Methodology

2.1. Study area

Sungo Bay is located in Shandong Province of People's Republic of China (Fig. 1). With an area of 180 km^2 and depths varying gradually until approximately 20 m at the sea boundary (Fig. 1), it has been used for aquaculture for more than 20 years (Guo et al., 1999). The main cultivated species include kelp (*Laminaria japonica*), oyster (*Crassostrea gigas*) and scallop (*Chlamys farreri*). Scallops and oysters are mostly contained in lantern nets and kelps are tied to ropes. One of the most limiting factors for bivalve culture in Sungo Bay is scallop mortality. High summer mortalities in recent years have led to changed aquaculture practices, including shifting the rearing periods. The main changes in those aquaculture practices, including areas of polyculture or monoculture, are summarised in Fig. 3. These show that the whole bay has been used for mariculture.

There is a considerable amount of water quality data for Sungo Bay. There were sampling campaigns in several stations over the bay in 1983–1984, 1989–1990, 1993–1994 and 1999–2000 (Gazeau and Bacher, unpublished). These authors analysed the temporal and spatial variability of several variables such as temperature, salinity, total suspended particulates, suspended organic matter, nutrients and phytoplankton. The main conclusion emerging from this data analysis was that temporal variability is more important than spatial variability in Sungo Bay. Ranges for temperature were from 2 to 26 °C, suspended particulate matter from 5 to over 100 mg l^{-1} with an average value of 22 mg l^{-1}, organic contents of that suspended particulate matter from 1 to over 50%, and chlorophyll abundance from 2 to 10 μg l^{-1} with an average value of 1.2 μg l^{-1}.

2.2. Model structure and implementation

The model developed for Sungo Bay is a 2D vertically integrated, coupled hydrodynamic–biogeochemical model. It is based on a finite difference bathymetric staggered grid (Vreugdenhil, 1989) with 1120 cells (32 columns × 35 lines) and a spatial resolution of 500 m (Fig. 1). The model time step is 36 s. However, due to the semi-implicit method used for time integrations, each time step is divided in two semi-time steps of 18 s. At every semi-time step, one of the speed components is calculated semi-implicitly and the other explicitly, on an alternating sequence. The model has a land and an ocean boundary. It is forced by tidal height at the sea boundary, light intensity, air temperature, wind speed, cloud cover and boundary conditions for some of the simulated state variables. It solves the general 2D transport equation (Eq. (1)) (Neves, 1985; Knauss, 1997). The hydrodynamic sub-model solves the speed components, whereas biogeochemical processes such as primary productivity and grazing, as well as physical processes such as sediment deposition and resuspension provide the 'sources' and 'sinks' terms of Eq. (1).

$$\frac{\mathrm{d}(hS)}{\mathrm{d}t} + \frac{\partial(uhS)}{\partial x} + \frac{\partial(vhS)}{\partial y} = \frac{\partial(Ah(\partial S/\partial x))}{\partial x} + \frac{\partial(Ah(\partial S/\partial y))}{\partial y} + \text{sources–sinks} \quad (1)$$

where h is the depth (m), u and v are current speeds in x and y directions (m s^{-1}), A is the coefficient of eddy diffusivity (m^2 s^{-1}), and S is a conservative (sources and sinks are null) or a non-conservative variable in the respective concentration units.

The model was implemented using EcoWin (Ferreira, 1995). EcoWin uses object-oriented programming (OOP) to relate a set of "ecological" objects by means of a server or shell which allows these to interact with each other, and displays the results of their interaction. Both the EcoWin shell and the objects have been programmed in C++ for

Table 1
EcoWin objects implemented for Sungo Bay (see text)

Object type	Object name	Object outputs
Objects acting as forcing functions	Wind object	Wind speed
	Air temperature object	Air temperature
	Water temperature object	Radiative balance between water and atmosphere and water temperature
	Light intensity object	Total and photosynthetically active radiation (PAR) at the surface and at any depth
	Tide object	Tidal height
Objects acting as state variables	Hydrodynamic 2D object	Sea level, current speed and direction
	Dissolved substances object	Dissolved inorganic nitrogen (DIN)
	Suspended matter object	Total particulate matter (TPM), particulate organic matter (POM) and the water light extinction coefficient
	Phytoplankton object	Phytoplankton biomass (PHY) and productivity
	Zooplankton object	Zooplankton biomass (ZOO) and productivity
	Laminaria japonica object	Kelp biomass and productivity
	Crassostrea gigas object	Oyster size, biomass, density, filtration, feeding, assimilation and scope for growth
	Chlamys farreri object	Scallops size, biomass, density, filtration, feeding, assimilation and scope for growth
	Man object	Harvest yields of kelps, oysters and scallops

Windows^{TM}. There are objects to represent the forcing functions and the different sets of state variables (Table 1). The objects are described below. The physical and biogeochemical processes simulated by the model are presented in Fig. 2. Differential equations used for suspended matter dynamics and biogeochemical processes are shown in Table 2 . They represent the sources–sinks terms of Eq. (1). The corresponding rate equations are presented in Table 3. In Table 4, the model parameters are listed.

2.2.1. Wind object

This object returns wind speed forcing variable average values to the water temperature object. These values are then used to calculate heat losses through evaporation.

2.2.2. Air temperature object

This object reads forcing variable air temperature values and returns them to the water temperature object, to be used to calculate sensible heat exchanges between the water and the atmosphere.

2.2.3. Light intensity and water temperature objects

Light intensity and water temperature were calculated by a light and a water temperature object using standard formulations described in Brock (1981) and Portela and Neves (1994). Submarine light intensity was computed from the Lambert–Beer law. The water light extinction coefficient was computed by the suspended matter object (see below).

2.2.4. Hydrodynamic object

The 2D barotropic hydrodynamic equations were adapted from Neves (1985). During each of the semi-time steps, the model calculates the velocity field with the equations of motion and the equation of continuity (Knauss, 1997), forced by tidal height at the sea boundary, and solving the transport equation (Eq. (1)) for all dissolved and suspended variables. The tidal forcing at the sea boundary was based on the lunisolar diurnal (K1) and the principal lunar (M2) harmonic constants (see below).

An eddy diffusivity of $100\,m^2\,s^{-1}$ was chosen according to the spatial scale of the model and to values used by other authors (e.g. Neves, 1985). Manning coefficients of 0.03 and 0.15 were used for non-aquaculture and aquaculture areas, respectively; as estimated for Sungo Bay, where aquaculture structures slow down the flow, reducing water exchange, and therefore with a potential impact on carrying capacity (Grant and Bacher, 2001).

Table 2
General differential equations for dissolved inorganic nitrogen, POM, phytoplankton and zooplankton

Dissolved inorganic nitrogen (DIN) (μmol N l^{-1})

$$\frac{\mathrm{dDIN}_{ij}}{\mathrm{d}t} = \mathrm{POMMiner}N_{ij} + \mathrm{ZOOExcr}N_{ij} + \mathrm{ZOOMort}N_{ij} + \mathrm{BIVExcr}N_{ij} + \mathrm{PHYMort}N_{ij} + \mathrm{PHYExud}N_{ij} - \mathrm{PP}N_{ij} + \mathrm{DINloads}_{ij} \quad (3)$$

$\mathrm{POMMiner}N_{ij}$	POM mineralisation[a] (μmol N l^{-1} per day)
$\mathrm{ZOOExcr}N_{ij}$	Zooplankton excretion[a] (μmol N l^{-1} per day)
$\mathrm{ZOOMort}N_{ij}$	Zooplankton mortality[a] (μmol N l^{-1} per day)
$\mathrm{BIVExcr}N_{ij}$	Scallop and/or oyster excretion[a] (μmol N l^{-1} per day)
$\mathrm{PHYMort}N_{ij}$	Phytoplankton mortality[a] (μmol N l^{-1} per day)
$\mathrm{PHYExud}N_{ij}$	Phytoplankton exudation[a] (μmol N l^{-1} per day)
$\mathrm{PP}N_{ij}$	Gross primary productivity of phytoplankton and kelps[a] (μmol N l^{-1} per day)
$\mathrm{DINLoads}_{ij}$	Nitrogen loads (μmol N l^{-1} per day)

Total (TPM) and organic (POM) particulate matter (mg l^{-1})

$$\frac{\mathrm{dTPM}_{ij}}{\mathrm{d}t} = \mathrm{TPMDep}_{ij} - \mathrm{TPMResus}_{ij} + \frac{\mathrm{dPHYTOT}_{ij}}{\mathrm{d}t} - \mathrm{POMMiner}_{ij} + \mathrm{TPMLoads}_{ij} \quad (4)$$

$$\frac{\mathrm{dPOM}_{ij}}{\mathrm{d}t} = \mathrm{POMDep}_{ij} - \mathrm{POMResus}_{ij} + \frac{\mathrm{dPHYORG}_{ij}}{\mathrm{d}t} - \mathrm{POMMiner}_{ij} + \mathrm{POMLoads}_{ij} \quad (5)$$

TPMDep_{ij}	TPM deposition rate (mg l^{-1} per day)
$\mathrm{TPMResus}_{ij}$	TPM resuspension rate (mg l^{-1} per day)
$\mathrm{dPHYTOT}_{ij}/\mathrm{d}t$	Net variation on phytoplankton biomass converted from carbon units (mg l^{-1} per day)
$\mathrm{TPMLoads}_{ij}$	TPM loads (mg l^{-1} per day)
POMDep_{ij}	POM deposition rate (mg l^{-1} per day)
$\mathrm{POMResus}_{ij}$	POM resuspension rate (mg l^{-1} per day)
$\mathrm{dPHYORG}_{ij}/\mathrm{d}t$	Net variation on phytoplankton organics (mg l^{-1} per day)
$\mathrm{POMMiner}_{ij}$	POM mineralisation (mg l^{-1} per day)
$\mathrm{POMLoads}_{ij}$	POM loads (mg l^{-1} per day)

Phytoplankton (μg C l^{-1})[b]

$$\frac{\mathrm{dPHY}_{ij}}{\mathrm{d}t} = \mathrm{PHY}_{ij}(\mathrm{PHYGPP}_{ij} - \mathrm{PHYExud}_{ij} - \mathrm{PHYResp}_{ij} - \mathrm{PHYMort}_{ij}) - \mathrm{Gz}_{ij}\mathrm{ZOO}_{ij}^{\mathrm{conv}}\mathrm{ZOO} - \mathrm{Gb}_{ij}\mathrm{BIV}_{ij}^{\mathrm{conv}}\mathrm{BIV} + \mathrm{PHYLoads}_{ij} \quad (6)$$

PHYGPP_{ij}	Gross primary productivity (per day)
$\mathrm{PHYExud}_{ij}$	Exudation rate (per day)
$\mathrm{PHYResp}_{ij}$	Respiration rate (per day)
$\mathrm{PHYMort}_{ij}$	Mortality rate (per day)
Gz_{ij}	Zooplankton grazing rate (per day)
Gb_{ij}	Bivalve grazing rate (per day)
$\mathrm{ZOO}_{ij}^{\mathrm{conv}}\mathrm{ZOO}$	Zooplankton biomass converted to carbon (μg C l^{-1} per day)
$\mathrm{BIV}_{ij}^{\mathrm{conv}}\mathrm{BIV}$	Bivalve biomass converted to carbon (μg C l^{-1} per day)
$\mathrm{PHYLoads}_{ij}$	Phytoplankton loads (μg C l^{-1} per day)

Laminaria japonica (g DW m^{-2})

$$\frac{\mathrm{dKELPS}_{ij}}{\mathrm{d}t} = r\mathrm{KELPS}_{ij}\, f(T)\, f(\mathrm{DIN}) + \mathrm{KELPSeed}_{ij} - \mathrm{KELPHarv}_{ij} \quad (7)$$

r	Net maximum growth rate (per day)
$f(T)$	Temperature limitation
$f(N)$	Nutrient limitation

Table 2 (*Continued*)

$KELPSeed_{ij}$	Kelp seed (g per day)
$KELPHarv_{ij}$	Kelp harvest (g per day)

Zooplankton (mg FW l^{-1})

$$\frac{dZOO_{ij}}{dt} = ZOO_{ij}(ZOORation_{ij} - ZOOResp_{ij} - ZOOMort_{ij} - ZOOExcr_{ij}) + ZOOLoads_{ij} \quad (8)$$

$ZOORation_{ij}$	Feeding rate (per day)
$ZOOResp_{ij}$	Respiration rate (per day)
$ZOOMort_{ij}$	Mortality rate (per day)
$ZOOExcr_{ij}$	Excretion rate (per day)
$ZOOLoads_{ij}$	Zooplankton loads (mg FW l^{-1} per day)

Bivalves (g DW m^{-2})

$$\frac{dBIV_{ij}}{dt} = BIVDens_{ij}(BIVAbsor_{ij} - BIVResp_{ij} - BIVExcr_{ij} - BIVMort_{ij}) + BIVSeed_{ij} - BIVHarv_{ij} \quad (9)$$

$BIVDens_{ij}$	Density (indiv. m^{-2})
$BIVAbsor_{ij}$	Absorption rate (g DW indiv.$^{-1}$ per day)
$BIVResp_{ij}$	Respiration rate (g DW indiv.$^{-1}$ per day)
$BIVExcr_{ij}$	Excretion rate (g DW indiv.$^{-1}$ per day)
$BIVMort_{ij}$	Mortality rate (g DW indiv.$^{-1}$ per day)
$BIVSeed_{ij}$	Seeding rate (g DW m^{-2} per day)
$BIVHarv_{ij}$	Harvest rate (g DW m^{-2} per day)

The subscripts i and j refer to the line and columns of the model grid. These differential equations only describe changes due to non-conservative processes and provide the sources–sinks terms of Eq. (1) (refer Section 2). The load terms refer to loads along the sea boundary.

[a] The rates are converted from different units to nitrogen. Conversion factors were taken from Parsons et al. (1984) and Jørgensen et al. (1991) (cf. Table 4).

[b] For output phytoplankton biomass is converted to chlorophyll, assuming a chlorophyll/carbon ratio of 0.02 (Jørgensen et al., 1991).

Table 3
Rate equations

TPM and POM

$$SinkingVelocity_{ij} = 100\exp(-0.000209\,DistanceFromSea) \quad (10)$$

$$TPMDep_{ij} = SinkingVelocity_{ij}\frac{TPM_{ij}}{Depth_{ij}} \quad (11)$$

$$TPMResus_{ij} = ErateVelocityShear_{ij} \quad (12)$$

if $\sqrt{Drag}|Speed| < CritSpeed$ then $VelocityShear_{ij} = 0$ else

$$VelocityShear_{ij} = \min\left(\frac{0.02^2}{(CritSpeed)^2} - 1.0, \frac{\left(\sqrt{Drag}|Speed|\right)^2}{(CritSpeed)^2} - 1.0\right) \quad (13)$$

0.02—threshold value to avoid very high resuspension rates (calibrated)

$$POMDep_{ij} = TPMDep_{ij}\frac{POM_{ij}}{TPM_{ij}} \quad (14)$$

$$POMResus_{ij} = TPMResus_{ij}\frac{POM_{ij}}{TPM_{ij}} \quad (15)$$

$$Drag = \frac{gn^2}{Depth^{1/3}} \quad \text{(calculated by the hydrodynamic object)} \quad (16)$$

Table 3 (*Continued*)

n	Manning coefficient	
g	Gravity ($m\,s^{-2}$)	
CritSpeed	Velocity threshold for resuspension ($m\,s^{-1}$)	

Phytoplankton

$$\mathrm{PHYGPP}_{ij} = P_{\max} f(I) f(T) f(\mathrm{DIN}) \quad (17)$$

$$f(I) = \frac{\exp(1)}{k\mathrm{Depth}} \left(\exp\left(\frac{I_z}{I_{\mathrm{opt}}}\right) - \exp\left(\frac{I_0}{I_{\mathrm{opt}}}\right) \right) \quad (18)$$

$$f(T) = e^{\alpha T} \quad (19)$$

$$f(\mathrm{DIN}) = \min(\mathrm{PHYGPP}_{ij}(I, T), \mathrm{PHYGPP}_{ij}(\mathrm{DIN})) \quad (20)$$

$$\mathrm{PHYExud}_{ij} = 0.05\mathrm{PHYGPP}_{ij} \quad (21)$$

$$\mathrm{PHYResp}_{ij} = \max(0.10\mathrm{PHYGPP}_{ij}, 0.02\mathrm{PHY}_{ij}) \quad (22)$$

$f(I)$	Light limitation function	Calculated
$f(T)$	Temperature limitation function	Calculated
f(DIN)	Nutrient limitation function	Calculated
$p_{\max}$	Maximum photosynthesis (per day)	
I_0 and I_z	Light intensities at grid cell top and bottom, respectively ($\mu E\,m^{-2}\,s^{-1}$)	Calculated
I_{opt}	Optimum light intensity ($\mu E\,m^{-2}\,s^{-1}$)	
α	Temperature augmentation rate ($^{\circ}C^{-1}$)	

Laminaria japonica

$$f(T) = \frac{2.0(1.0 + \mathrm{Betat})X_t}{X_t^2 + 2.0\mathrm{Betat}X_t + 1.0} \quad (23)$$

where

$$X_t = \frac{T_w - T_s}{T_s - T_e} \quad (24)$$

f(DIN) calculated as for phytoplankton

T_w	Water temperature ($^{\circ}C$)
T_s	Optimal temperature ($^{\circ}C$)
T_e	Lethal temperature ($^{\circ}C$)
Betat	Adjustment parameter

Zooplankton

if $\mathrm{PHY}_{ij} < \mathrm{PHYmin}$, $\mathrm{ZOORation}_{ij} = 0$ else

$$\mathrm{ZOORation}_{ij} = R_{\max}(1 - \exp(\mathrm{Kgraze}(\mathrm{PHYmin} - \mathrm{PHY}_{ij}))) \quad (25)$$

$R_{\max}$	Maximum ration (per day)
Kgraze	Adjustment parameter
PHYmin	Phytoplankton threshold for feeding ($\mu g\,C\,l^{-1}$)

2.2.5. Tide object

This object uses the equations described in SHOM (1984) and the harmonic components M2 and K1 listed in Table 5 to calculate water level at the sea boundary. The values for these components were determined by Wan (personal communication) with a hydrodynamic model for the Bohai Sea (Table 5). According to Wan (personal communica-

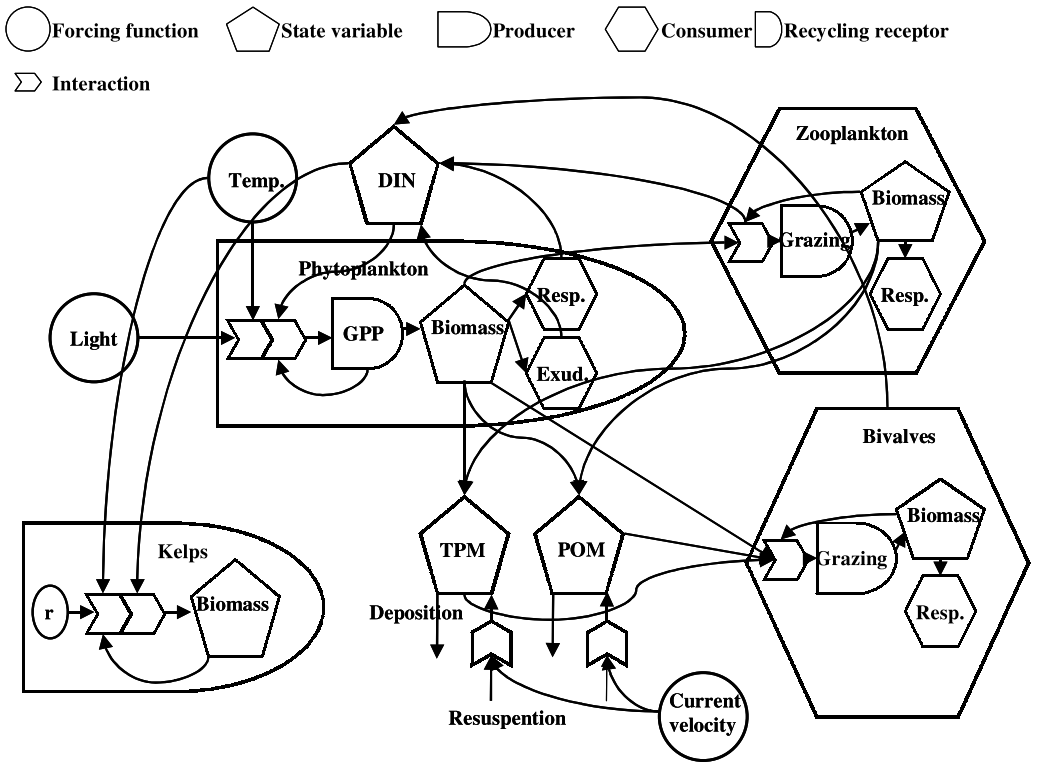

Fig. 2. Model diagram following the "energy circuit language" (Odum, 1973, 1983) (GPP, gross primary productivity; Resp., respiration; Exud., exudation; r, intrinsic rate of increase).

tion), north–south gradients along the sea boundary for the amplitude and phase of M2 approximate 4.2 mm km^{-1} and 0.4° km^{-1}, respectively. These gradients were considered in the model. Since the M2 component shifts with latitude, the object predicts a north–south total slope in sea level of approximately 1 cm. Boundary water levels are returned to the hydrodynamic object, where they are used to calculate the propagation of the tidal wave into the bay.

2.2.6. Dissolved substances object

The concentration of dissolved inorganic nitrogen (DIN) in each of the model grid cells was calculated as a function of biogeochemical and transport processes, including exchanges with the sea (Table 2). The DIN sinks were phytoplankton and kelp productivities. The sources were mineralisation of organic detritus, including dead phyto and zooplankton, as well as excretion processes (Table 2). A constant mineralisation rate was assumed (Table 4).

2.2.7. Suspended matter object

This object computed total particulate matter (TPM; in mg l^{-1}) and particulate organic matter (POM; in mg l^{-1}) from deposition and resuspension rates, from the exchanges with the sea and with other boxes (transport by the hydrodynamic object), and from the net contribution of phytoplankton biomass (Table 2). It also computed the mineralisation of POM, returning the resulting inorganic nitrogen to the dissolved substances object (see above). For this calculation, the nitrogen contents of POM and its mineralisation rate were assumed constant (Table 4).

Deposition of TPM in each grid cell was based on sinking velocity and cell depth, returned by the hydrodynamic object. Sinking velocity was calculated as a decaying exponential function with distance from the sea boundary, varying from 100 till less than 12 m per day (calibrated) (Table 4). This function was chosen to produce faster deposition rates at the higher energy areas where sediments are generally sands, compared

Table 4
Model parameters and conversion factors

Object	Parameter	Value	Reference
Hydrodynamic 2D object	Manning coefficient ($s\,m^{-1/3}$)	0.03–0.015	Grant and Bacher (2001)
	Eddy diffusivity	$100\,m^2\,s^{-1}$	Neves (1985)
Suspended matter object	CritSpeed	$0.00773\,m\,s^{-1}$	Calibrated
	Mineralisation rate of POM	0.05 per day	Jørgensen et al. (1991)
	Nitrogen contents of POM	0.08 (proportion of mass)	Jørgensen et al. (1991)
	Erate	$259.2\,g\,m^{-2}$ per day	Calibrated
Phytoplankton object	P_{max}	1.2 per day	Estimated
	I_{opt}	$491.4\,\mu E\,m^{-2}\,s^{-1}$	Estimated
	α	$0.017\,^{\circ}C^{-1}$	Estimated
	$PHYMort_{ij}$	0.05 per day	Jørgensen et al. (1991)
Laminaria japonica object	C/biomass ratio	0.26	Deslous-Paoli (personal communication)
	N/biomass ratio	0.16	Deslous-Paoli (personal communication)
	r	0.04 per day	Mao et al. (1993)
	T_s	13 °C	Petrell et al. (1993)
	T_e	25 °C	Petrell et al. (1993)
	Betat	3	Andersen and Nival (1989)
Zooplankton object	Dry weigh to fresh weight	5	Jørgensen et al. (1991)
	C/biomass ratio	0.3	Jørgensen et al. (1991)
	N/biomass ratio	0.05	Jørgensen et al. (1991)
	R_{max}	3 per day	Parsons et al. (1984)
	Kgraze	0.0005	Calibrated
	PHYmin	$40\,\mu g\,C\,l^{-1}$	Parsons et al. (1984)
	$ZOOResp_{ij}$	0.75 per day of absorbed food	Parsons et al. (1984)
	$ZOOExcr_{ij}$	0.1 per day of absorbed minus metabolised food	Calibrated
	$ZOOMort_{ij}$	0.05 per day	Calibrated

Most values were averaged from ranges reported by the stated authors.

with sheltered areas where fine sands are more common.

Resuspension of TPM in each grid cell was calculated as a function of current velocity and bottom drag, returned by the hydrodynamic object (Table 4).

Table 5
Harmonic constants (range in the case of M2) used at the sea boundary

	Amplitude (mm)	Phase (°)
K1	250	330
M2	600–650	25–30

The amplitude and phase of the component M2 shifts in the north–south direction at a rate of $4.2\,mm\,km^{-1}$ and $0.4^{\circ}\,km^{-1}$, respectively, following Wan (personal communication) (refer Section 2).

Below a critical velocity value, resuspension does not occur. Above a certain threshold for the product of bottom drag times current velocity (velocity shear), resuspension was assumed constant. This is to avoid unrealistically high resuspension rates. This object was partly based on a Stella model developed by Grant and Bacher (unpublished).

Deposition and resuspension of POM was calculated from deposition and resuspension of TPM times the POM/TPM ratio at each grid cell (Table 4).

The light extinction coefficient (k in m^{-1}) was calculated from an empirical relationship with TPM (Eq. (2)), obtained from historical data for Sungo Bay (Bacher, personal communication):

$$k = 0.0484\,\mathrm{TPM} + 0.0243 \quad (2)$$

2.2.8. Phytoplankton object

Phytoplankton biomass in each of the model grid cells was calculated as a function of physiological, demographic and transport processes, including exchanges with the sea (Table 2). Primary productivity was estimated from light intensity, temperature and nutrient data delivered by the respective objects (Table 4). If the dissolved substances object was not activated by the user, then primary production was calculated solely as a function of light and temperature.

The light function was taken from Steele (1962) and integrated over depth (Table 3). Temperature limitation was based on Eppley (1972) (Table 4). The parameters of both functions (Table 4) were estimated using the non-linear regression Newton method from productivity measurements carried out in Sungo Bay with the C^{14} technique. It was not possible to combine these limitation functions with a Michaelis–Menten function for nutrient limitation, and still get realistic estimates for the light and temperature parameters. Therefore, nutrient limitation was calculated from the following assumptions:

(1) DIN was assumed to be the limiting nutrient. This assumption was based on the water N/P ratios observed in Sungo Bay from 1983 till 1994. From 193 samples when primary productivity was also measured, the N/P atomic ratio in seawater averaged 4.1, and was less than 16 in 187 of those samples.
(2) When phytoplankton productivity calculated from light and temperature could not be supported by available DIN to keep the C/N ratio within its default value (6.6), productivity was reduced in order to keep the mentioned ratio constant. This was to avoid unrealistic C/P cell ratios. This assumption implies that phytoplankton may efficiently use the available DIN, and that the cell quotas for N and C remain constant, which may on average be true.

Phytoplankton respiration was calculated by removing a constant proportion of the fixed carbon, thus converting the phytoplankton gross primary production (GPP) into net primary production (NPP). This has been defined from a range of values for algal respiration and primary production given by Jørgensen et al. (1991). When GPP was zero, respiration was calculated as a constant fraction of biomass (Table 3).

2.2.9. Zooplankton object

Zooplankton biomass in each of the model grid cells was calculated as a function of physiologic, demographic and transport processes, including exchanges with the sea (Table 2). Feeding was calculated using an Ivlev equation (Table 3) (Parsons et al., 1984).

2.2.10. Laminaria japonica object

Kelp growth rate was assumed to be limited by temperature and DIN. Light was not considered a limiting factor because kelp culture ropes can be adjusted up or down to overcome light limitation. Kelp is allowed to grow until a threshold biomass that corresponds to a value of 80 g individual DW. The function used for temperature limitation is from Andersen and Nival (1989) following Gazeau (2000) (Table 3). The function used for nutrient limitation was the same as described previously for phytoplankton.

2.2.11. Chlamys farreri (scallops) and Crassostrea gigas (oyster) objects

The equations and parameters used for scallop growth are described elsewhere (Hawkins et al., 2001, 2002). These were obtained and calibrated from experimental work undertaken in Sungo Bay. They include selective feeding processes, taking into account the available TPM, detrital POM and phytoplankton POM. Temperature limitations of both feeding and respiration are also considered. The model computes growth of shell and soft tissue.

The equations and parameters used for oyster growth are based on those described in Barillé et al. (1997). These equations also include selective feeding processes, by separately calculating the production of mineral and organic matter in pseudofaeces.

Both the scallop and the oyster objects tend to reduce POM concentration, but their excretion is a positive feedback to phytoplankton and kelp productivities. These objects depend on the Man object (see below) for seeding small spat and for harvesting commercial sized individuals.

The objects include empirical equations to relate shell length with shell weight. This is because harvest by the Man object (see below) depends not only on available biomass but also on size. If bivalves are below the commercial size, harvest does not occur. The commercial size was 6 cm for scallops under the 1993–1994 scenario. It was reduced to 5 cm in

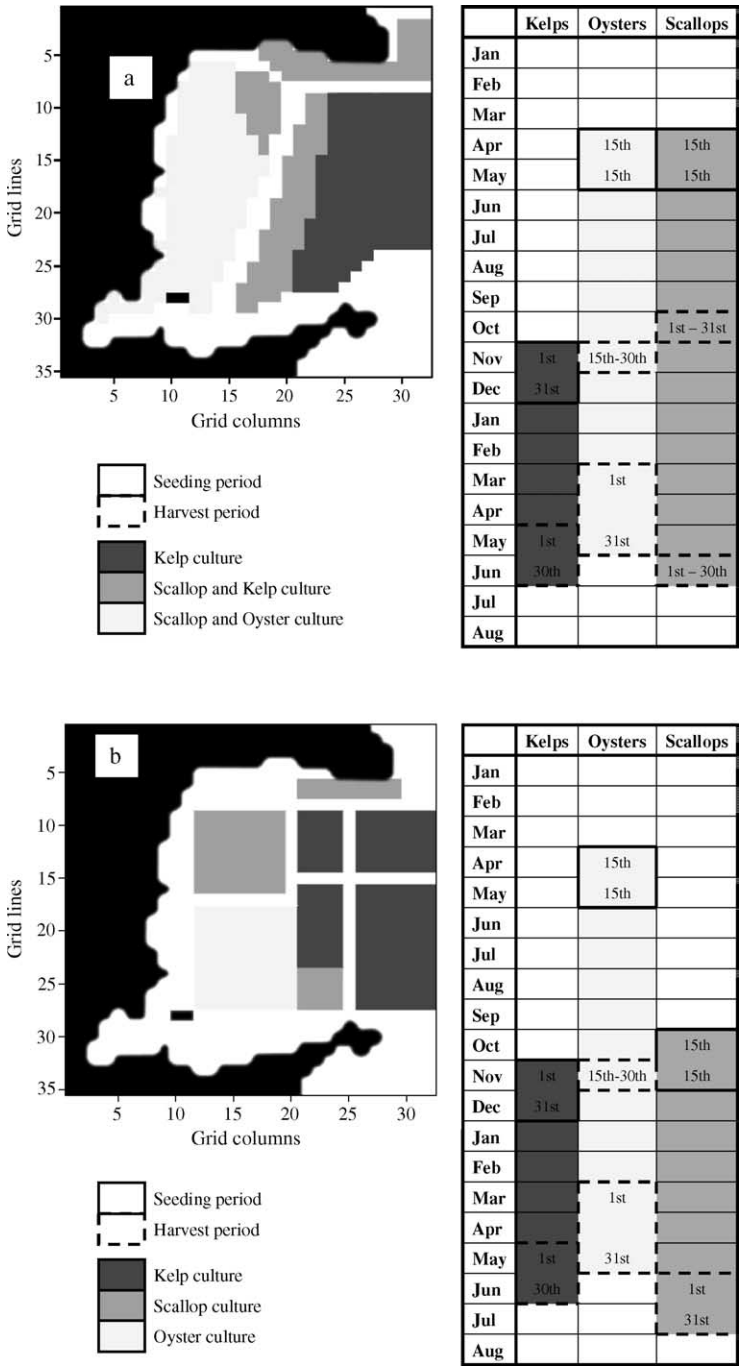

	Kelps	Oysters	Scallops
Jan			
Feb			
Mar			
Apr		15th	15th
May		15th	15th
Jun			
Jul			
Aug			
Sep			
Oct			1st – 31st
Nov	1st	15th-30th	
Dec	31st		
Jan			
Feb			
Mar		1st	
Apr			
May	1st	31st	
Jun	30th		1st – 30th
Jul			
Aug			

	Kelps	Oysters	Scallops
Jan			
Feb			
Mar			
Apr		15th	
May		15th	
Jun			
Jul			
Aug			
Sep			
Oct			15th
Nov	1st	15th-30th	15th
Dec	31st		
Jan			
Feb			
Mar		1st	
Apr			
May	1st	31st	
Jun	30th		1st
Jul			31st
Aug			

Fig. 3. (a) 1993–1994 and (b) 1999–2000 aquaculture scenarios. On the left, spatial distribution of the different cultures. On the right, seeding and harvesting periods for the cultivated species. Kelp density: 12 indiv. m^{-2}; oyster and scallop densities: 59 indiv. m^{-2}; oyster and scallop commercial sizes: 7 and 6 cm (5 cm in the 1999–2000 scenario) shell length, respectively.

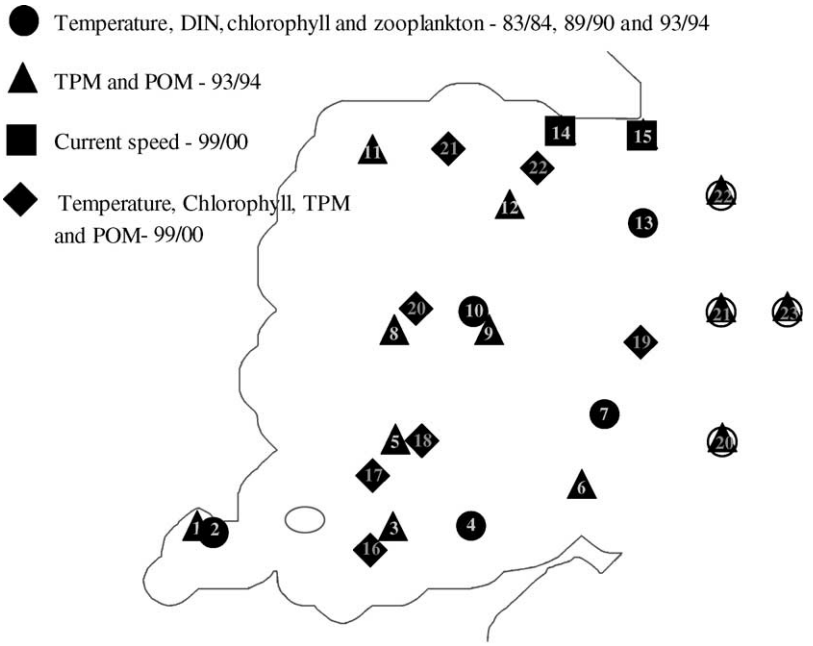

Fig. 4. Location and codes of sampling stations used for boundary conditions, model calibration and validation. Stations were chosen according to available data (refer Section 2).

1999–2000. For the oysters, the commercial size was 7 cm.

The dependence of mortality on stock density was not considered due to the lack of experimental data, despite some evidence for density-dependent mortality (Fang, unpublished data). A constant mortality rate of 10% over the rearing period was assumed for the oysters. For the scallops, an annual value of 23% was adopted, but with 20% occurring during August and September, when water temperature is highest. These values were obtained both from empirical estimates and discussion with farmers.

2.2.12. *Man object*

This object simulates seeding and harvesting of kelps, oysters and scallops. The model may be initialised with or without any of these species. Alternatively, seeding and harvesting may be simulated by the Man object at any date. Dates chosen for the present simulations represent the different aquaculture scenarios as summarised in Fig. 3.

Table 6
Aquaculture scenarios simulated with the model (cf. Sections 2 and 2.3, Fig. 3)

Aquaculture scenarios	Aquaculture zones			Culture densities		
	Kelps	Scallops	Oysters	Kelps (indiv. m^{-2})	Scallops (indiv. m^{-2})	Oysters (indiv. m^{-2})
I	See Fig. 3	See Fig. 3	See Fig. 3	12	59	59
IIa	See Fig. 3	See Fig. 3	See Fig. 3	12	59	59
IIb	See Fig. 3	See Fig. 3	See Fig. 3	12	29.5	29.5
Iic	See Fig. 3	See Fig. 3	See Fig. 3	12	118	118
Iid	See Fig. 3	See Fig. 3	See Fig. 3	12	177	177
Iie	See Fig. 3	See Fig. 3	See Fig. 3	12	59	118
III	See Fig. 3	See Fig. 3	See Fig. 3	12	19	59

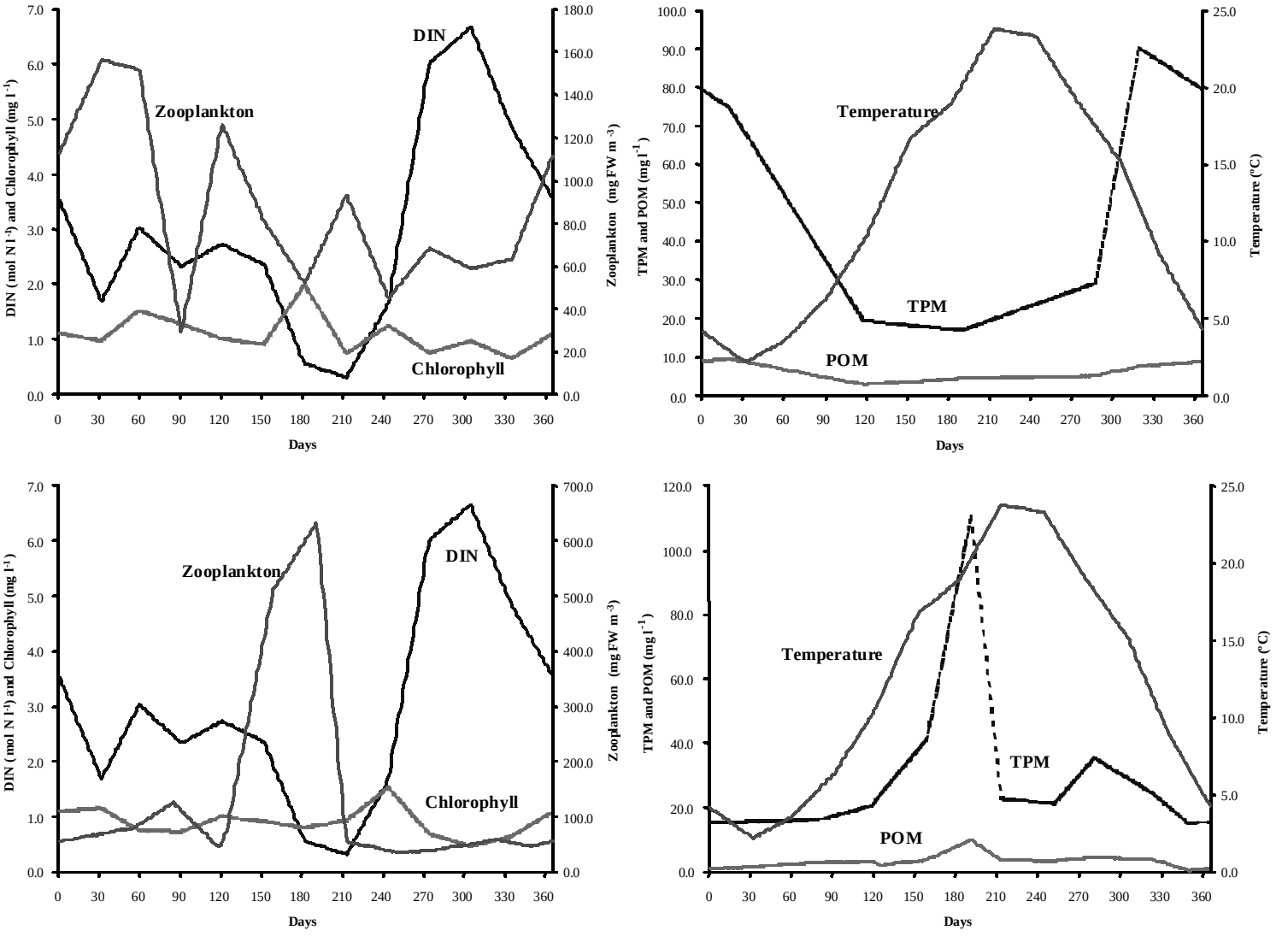

Fig. 5. Model boundary conditions for I (top charts) and IIa (bottom charts) aquaculture scenarios (refer Section 2) (cf. Table 6).

2.3. Model simulations

Seven scenarios were simulated in Sungo Bay, hereafter referred to as scenarios I, IIa, IIb, IIc, IId, IIe and III. Each scenario represented the whole cultivation cycle, starting in March and ending in July of the second year, depicting different spatial distributions and/or densities of the main cultivated species (Fig. 3a and b and Table 6), according to recent changes in aquaculture practice (refer above), including hypothetical variations that were designed to achieve the stated objectives (refer Section 1 and objectives). Scenarios can be divided as follows:

(i) culture practice implemented up to and during 1993–1994 (scenario I) (Fig. 3a and Table 6), with a initial stock of 4500, 0.3 and 1120 tons DW of kelps, oysters and scallops, respectively;
(ii) current culture practice, implemented in 1999–2000 (scenario IIa), with a initial stock of 2850, 0.6 and 1860 tons DW of kelps, oysters and scallops, respectively, and hypothetical variations in scallop and oyster densities, whilst maintaining seeding periods and spatial distributions as in scenario IIa (scenarios IIb–e) (Fig. 3b and Table 6); and
(iii) given apparent limitations on harvest yield for scallops (refer Section 3), a hypothetical scenario to assess whether scallop production might be increased without changing bivalve loads, in which the total quantity of scallops and oysters remained the same as in scenario IIa, but when the scallops were distributed over a larger area that covered the former cultivation areas for both scallops and kelp, thereby creating areas of combined kelp and scallop culture, whilst reducing the average scallop density from 59 to 19 indiv. m^{-2} (Fig. 3b and Table 6).

In spite of the amount of available data for Sungo Bay, most of it was not collected with the objective of developing a mathematical model. Different variables have been sampled with variable intensities over the years. For example, there is considerably less data on suspended particulate matter than on phytoplankton or dissolved nutrients. Further, we would have liked more information on forcing functions and boundary conditions. The latter had to be defined on the basis of data available for the most outer stations (Fig. 5). Temporal linear interpolations were carried out in order to obtain yearly time series for temperature, TPM, POM, DIN, chlorophyll and zooplankton (Fig. 5). Two sets of boundary conditions were used for the two aquaculture scenarios (Figs. 3 and 5). To reduce the length of the interpolation intervals to no more than one month, data from different years had to be combined. Therefore, the boundary conditions obtained are not representative of any particular year, but a mixture of different years, except for the 1999–2000 scenario, where a complete set of TPM, POM and chlorophyll data was available. Even in this case, conditions were defined by limited data that are hardly representative of the whole boundary. Sampling points used for boundary conditions, model calibration and validation are shown in Fig. 4. In so far as was possible, these points were chosen to maximise the number of measurements for comparison with model outputs.

Given that available data were limited, our main objective for calibration was to achieve predictions within the range of observed values. As such, the value of this model is in helping to synthesise most knowledge of ecology in Sungo Bay, and as a step towards a fully diagnostic tool for aquaculture management.

The model was calibrated with data collected until 1994. Simulations were then carried out under scenario IIa for validation. The overall correspondence between observed and predicted values was analysed with Model II linear regression analysis, following Laws and Archie (1981), with the major axis regression method as recommended by Mesplé et al. (1996) and described in Sokal and Rohlf (1995). ANOVA was used to test the significance of slopes and *y*-intercepts obtained, including the variance explained by the model. When the slope is not significantly different (S.D.) from 1 and the *y*-intercept not S.D. from 0, there is a good agreement between model and observations. When the *y*-intercept is S.D. from 0, there is a constant difference between model and observations. When the slope is not S.D. from 1 but S.D. from 0, the differences between model and observations are proportional to the value of the variable, but the model may explain a significant proportion of total variance. Given gaps in the historical data from Sungo Bay, these analysis were carried out only with the 1999–2000 data sets, with results obtained in seven sampling points over the bay for water quality data and one point for current speed data (cf. Fig. 4).

3. Results and discussion

Variations in the available data mean that the number of comparisons between field measurements and model predictions are different between the 1993–1994 and 1999–2000 aquaculture scenarios, and also among some of the variables within each scenario. The figures presented are just a sample of the comparisons performed, and were selected to represent the most inner parts of the bay, the middle and the outer areas.

3.1. Calibration and validation results—simulations I and IIa

3.1.1. Current speeds

The results of the hydrodynamic object were checked against real data at two different times and two different places. Comparisons were also made with findings from Grant and Bacher (2001), who modelled the potential impact of aquaculture structures on current flow and direction. Fig. 6 illustrates a comparison under the 1993–1994 scenario between current speed measurements and model results at sampling point 14. There is a close agreement between predicted and observed data. A further comparison is illustrated under the 1999–2000 scenario for two measurements at sampling point 14, one inside the northern-most aquaculture area and the other outside of that area in the navigation channel (Fig. 7). There is a reasonable similarity between predicted and observed values. Confirming this, the slopes of the Model II regressions between predicted and observed values were not S.D. from 1 and the *y*-intercepts were not S.D. from 0 ($P < 0.05$). The lack of current velocity data at other points of the bay prevented more comparisons. The difference between the current speeds inside and outside the aquaculture area may be as high as 50%, as is with the use of different Manning coefficients.

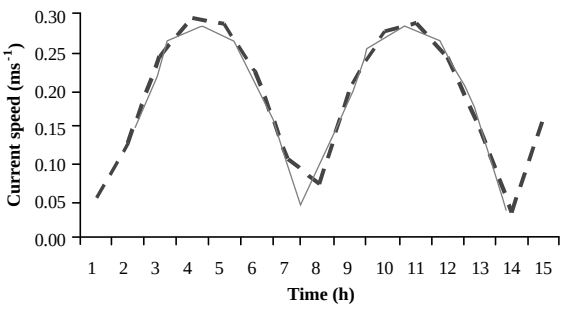

Fig. 6. Current speeds predicted by the model (broken line) and measured (solid line) at sampling point 15 (cf. Fig. 4) (data from Zhao et al., 1996), under scenario I (cf. Table 6).

In Fig. 8, vector plots are shown for the 1993–1994 and 1999–2000 scenarios, showing the major patterns of current circulation in Sungo Bay. There is a dominant gyre circulation, with higher current speeds near the mouth of the bay. During high water, the gyre is counter-clockwise, whereas during low tide there is a clockwise circulation.

Simulations were also carried out assuming a constant Manning coefficient of 0.03, to compare with the results obtained by Grant and Bacher (2001). The average current speed obtained over the whole bay for a 4-day simulation was $0.12\,m\,s^{-1}$, with a maximum of $0.59\,m\,s^{-1}$. With the two different Manning coefficients, an average of $0.06\,m\,s^{-1}$ was obtained, with a maximum of $0.46\,m\,s^{-1}$. This represents a 50% decrease in average current speed, caused by increased drag due to aquaculture structures, and shows the importance of having experimental estimates of the Manning coefficient. It is worth noting that the maximum values obtained by Grant and Bacher (2001) both with constant (0.03) and variable Manning coefficients (0.03 or 0.15) were a bit lower (0.5 and $0.3\,m\,s^{-1}$) than those obtained in the present work. However, the results are not fully comparable, due to the different distribution of aquaculture during our respective studies. In addition, the Aquadyn (Hydrosoft Energy; see http://www.hydrosoftenergie.com) model used by Grant and Bacher (2001) is based on a finite element integration scheme, whereas the model used in the present study is based on a finite difference scheme. In spite of these differences, the predicted circulation patterns are quite similar. Another comparison was made with the three-dimensional hydrodynamic model of Wan (2001), showing very similar current patterns and current speeds.

3.1.2. Water temperature

Observed and predicted temperatures are shown in Fig. 9. The model successfully simulates variations in observed temperature over the year and over space,

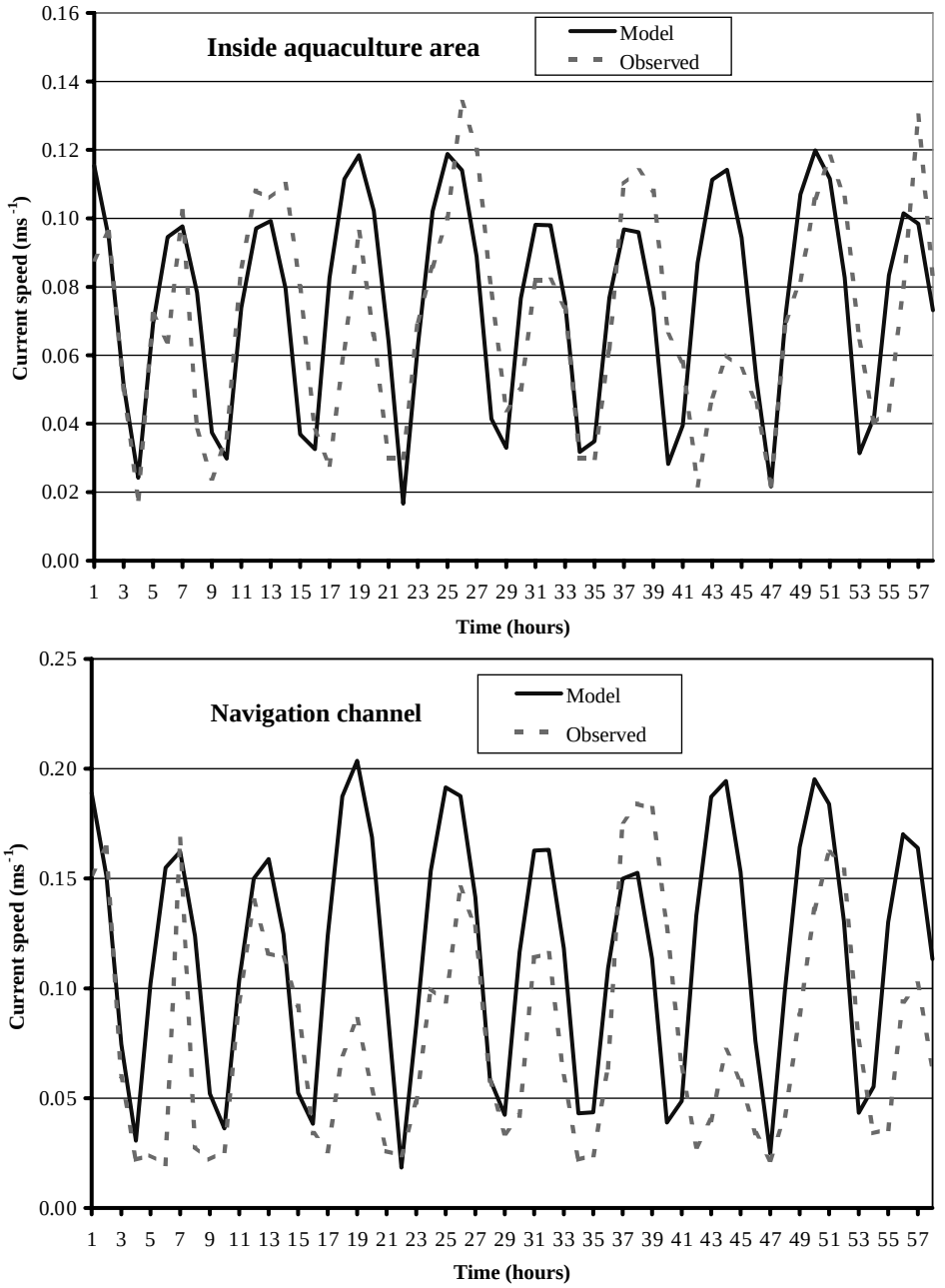

Fig. 7. Current speeds measured and predicted by the model and at sampling point 14 (cf. Fig. 3), under scenario IIa (cf. Table 6). Upper figure represents values measured or predicted in the most northern scallop cultivation area (cf. Fig. 3). Lower figure represents values measured or predicted in the navigation channel (cf. Fig. 3).

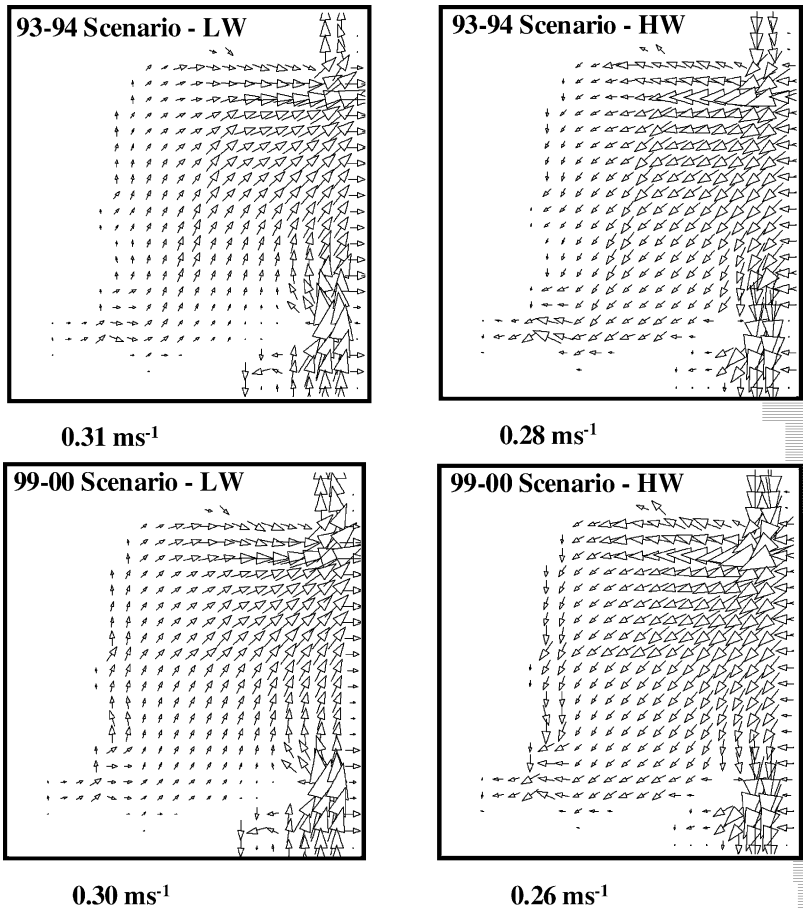

Fig. 8. Vector plots obtained with the model for the scenarios I and IIa (cf. Table 6) during low (LW) and high tides (HW) (refer Section 2). Maximum current speeds indicated close to each scenario.

with minimum values around 2 °C during winter and maximum values around 25 °C during August and September. The slope of the Model II regression between predicted and measured values was not significantly different from 1 and the *y*-intercept was not S.D. from 0 ($P < 0.05$).

3.1.3. DIN

DIN observed over several years (1983–1984, 1989–1990 and 1993–1994) is compared with model predictions under the 1993–1994 scenario in Fig. 10. Due to several data gaps during the 1993–1994 period, the boundary condition for DIN had to be averaged using measures obtained over several years. This limited the effectiveness of our model calibration. Nevertheless, model results are in general well within the range of observed values. It is difficult to identify clear temporal patterns, since during different years, maximum and minimum DIN values occurred in different seasons. However, in general, higher values occurred later in the year as are predicted by the model. With respect to the 1999–2000 period, too many nitrate values were missing to allow any reasonable comparison between observations and model predictions.

3.1.4. Phytoplankton

Chlorophyll concentrations observed are compared with model predictions under the 1993–1994 and the 1999–2000 scenarios (I and IIa) in Fig. 11. In general,

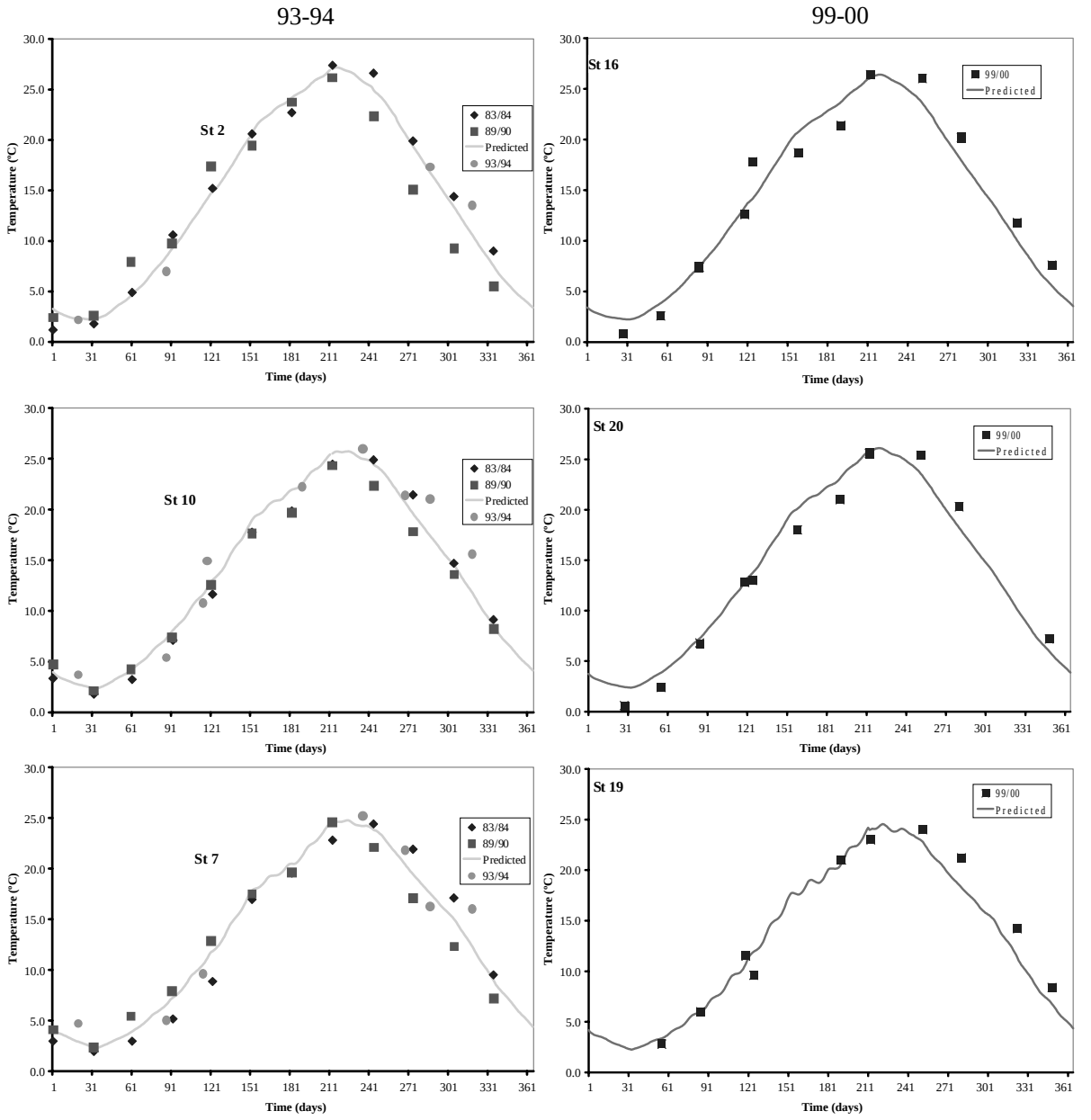

Fig. 9. Observed and predicted temperatures at some of the stations depicted in Fig. 4, for the scenarios I and IIa (cf. Table 6). Left charts correspond to scenario I and right charts to scenario IIa. From top to bottom, results correspond to stations at decreasing distances from the sea.

model predictions are well within the range of observed values. Again, as in the case of DIN, model calibration was complicated by several data gaps during the 1993–1994 period, such that the boundary condition for chlorophyll had to be averaged using results obtained over several years. Also, as for DIN, it is difficult to identify clear patterns over time, since during different years, maximum and minimum values

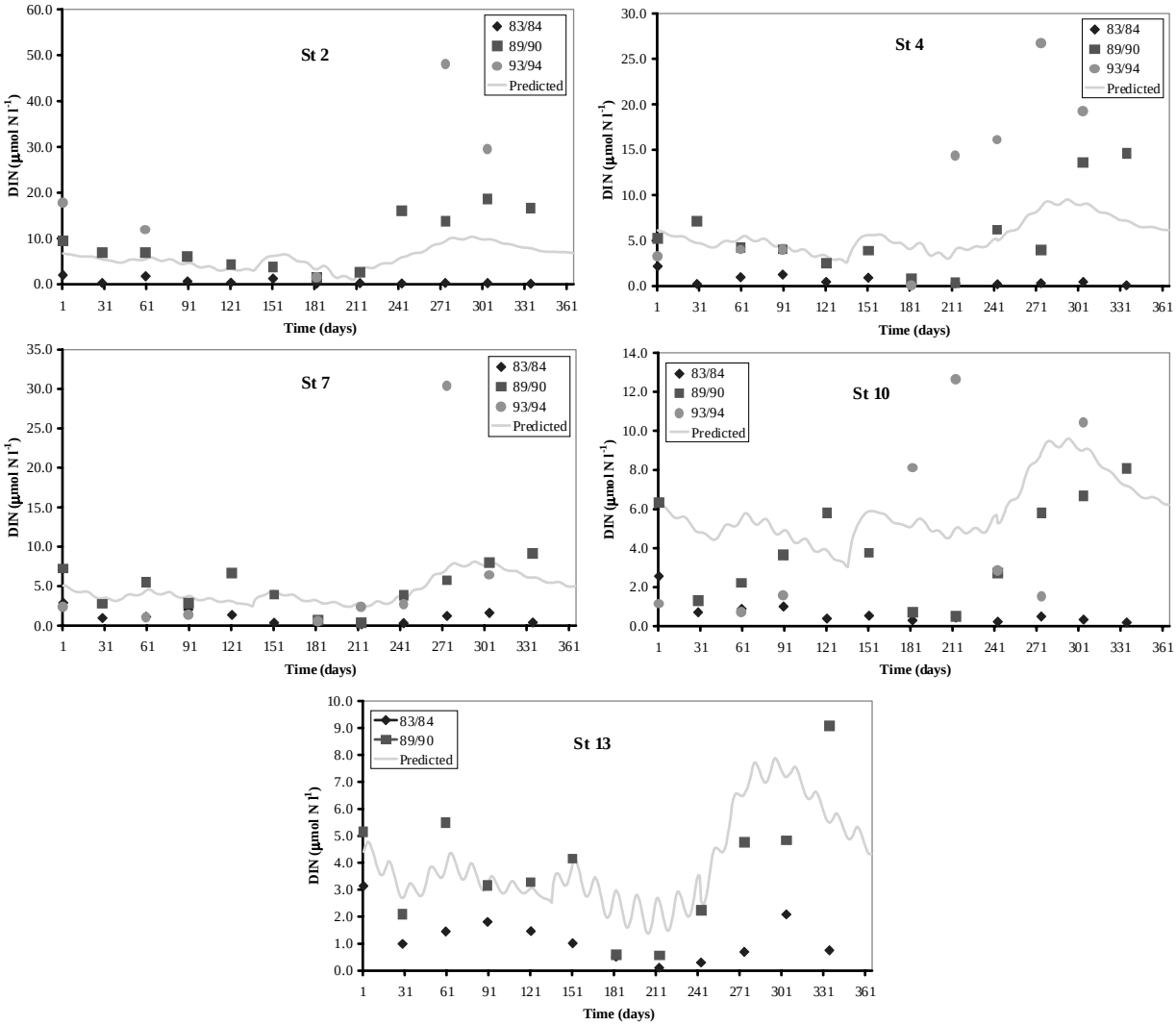

Fig. 10. Scenario I (cf. Table 6): observed and predicted DIN concentrations at some of the stations depicted in Fig. 4. From top to bottom, results correspond to stations at decreasing distances from the sea.

occurred in different seasons. Nevertheless, the model predicts two main maxima, one at the end of winter and the other during summer. The latter reflects a similar peak in the boundary condition (Fig. 5). The former appears associated with a seasonal reprieve from light and/or temperature limitations. Comparison of model outputs indicates that throughout this period, phytoplankton was not limited by nutrients.

Model predictions for the scenario IIa are generally within the range of observed values (Fig. 11). Two peaks predicted by the model in spring and summer match two similar peaks in the boundary condition (Fig. 5). Both occur approximately a month latter than in the 1993–1994 simulation. During the first-half of the year, the model tends to overestimate observations. There is a closer similarity between predicted and observed patterns during the second-half of the year. Predictions for those areas located near the boundary are better than for the inner stations. The slope of the Model II regression between measured and observed

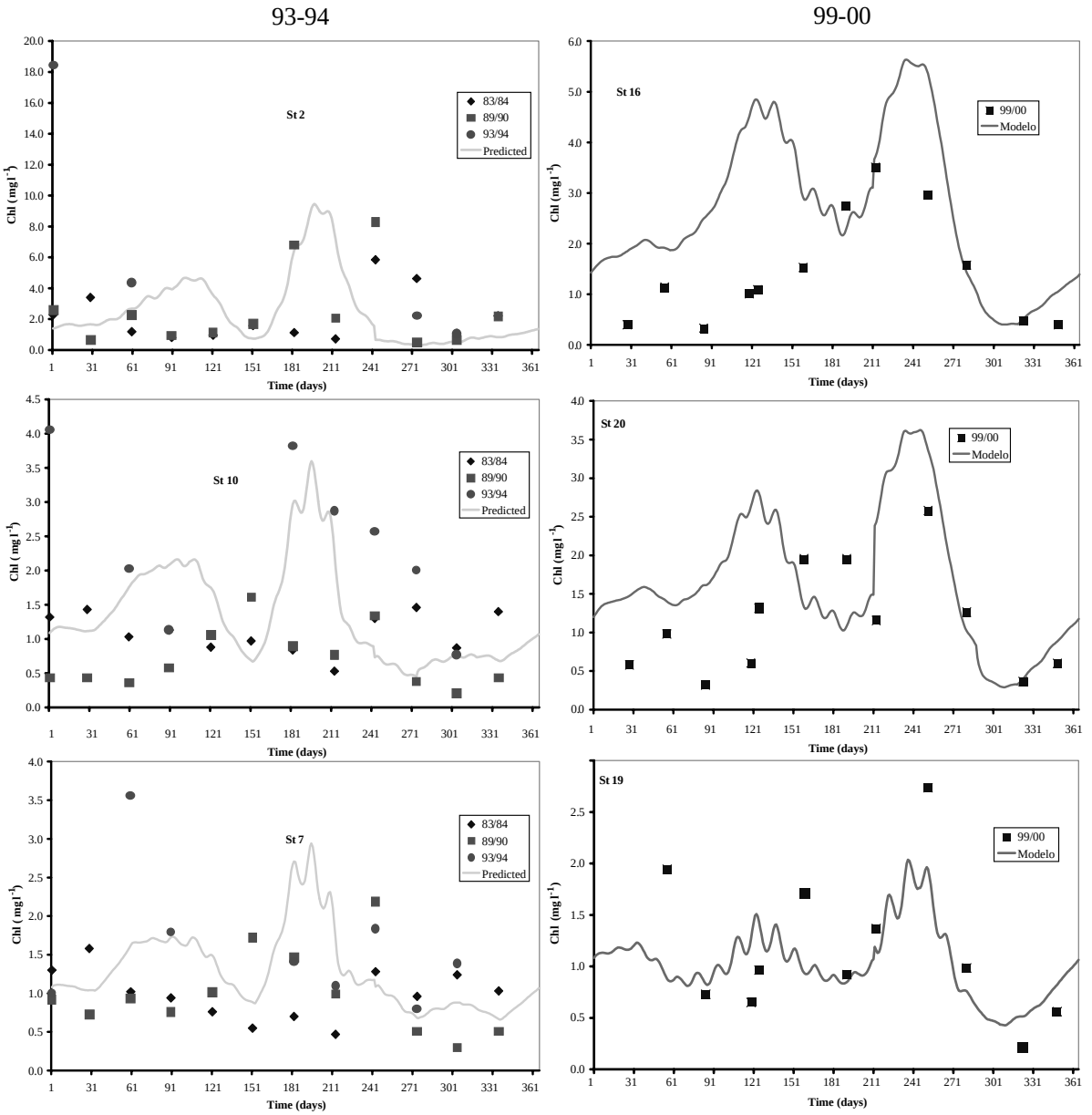

Fig. 11. Observed and predicted chlorophyll concentrations at some of the stations depicted in Fig. 4, for the scenarios I and IIa (cf. Table 6). Left charts correspond to scenario I and right charts to scenario IIa. From top to bottom, results correspond to stations at decreasing distances from the sea.

values was S.D. from 0, whereas the *y*-intercept was not S.D. from 0 ($P < 0.05$). The variance explained by the model was significant ($P < 0.01$). However, the slope was significantly lower than 1 ($P > 0.05$). These results imply that the model explains a significant proportion of the observed variance, but the differences between model and observations are proportional to the chlorophyll concentration (Mesplé et al., 1996).

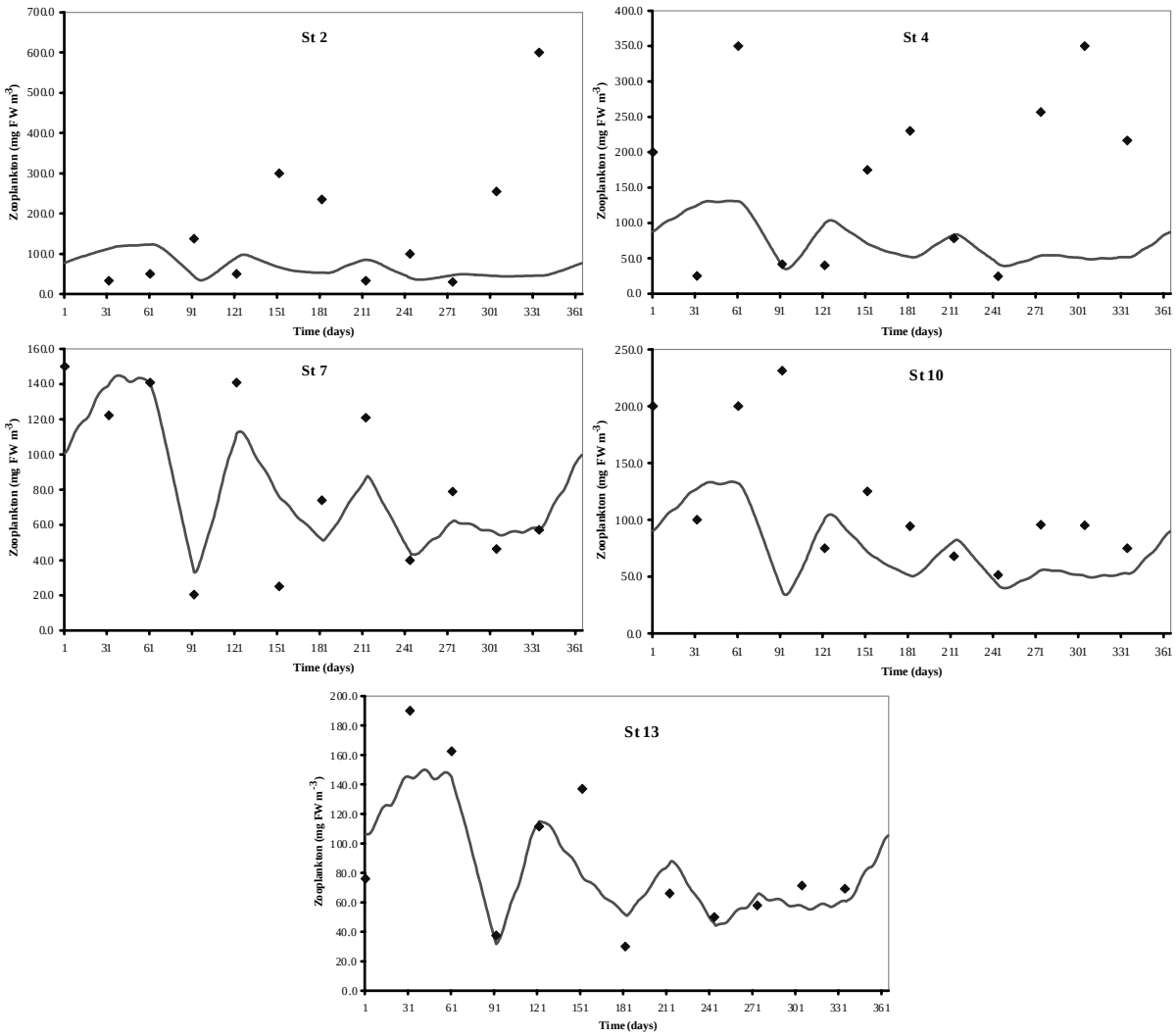

Fig. 12. Scenario I (cf. Table 6): observed (diamonds) and predicted (line) zooplankton concentrations at some of the stations depicted in Fig. 4. From top to bottom, results correspond to stations at decreasing distances from the sea.

3.1.5. Zooplankton

Measured zooplankton concentrations are compared with model predictions during the 1993–1994 period in Fig. 12. With the exception of the most inner station considered, the model results follow the expected patterns and are well within the range of observations. Model predictions could not be compared with measurements during the 1999–2000 period, because zooplankton had been collected by sieving through different-sized nets.

3.1.6. TPM and POM

Measured concentrations of TPM and POM are compared with model predictions from scenarios I and IIa in Fig. 13. During the 1993–1994 period, samples were collected with intervals of more than one month, thus posing difficulties both in defining the boundary conditions and for calibrating the model. Whilst Fig. 13 illustrates the high temporal variability of both variables, model predictions generally fall within the observed range of concentrations.

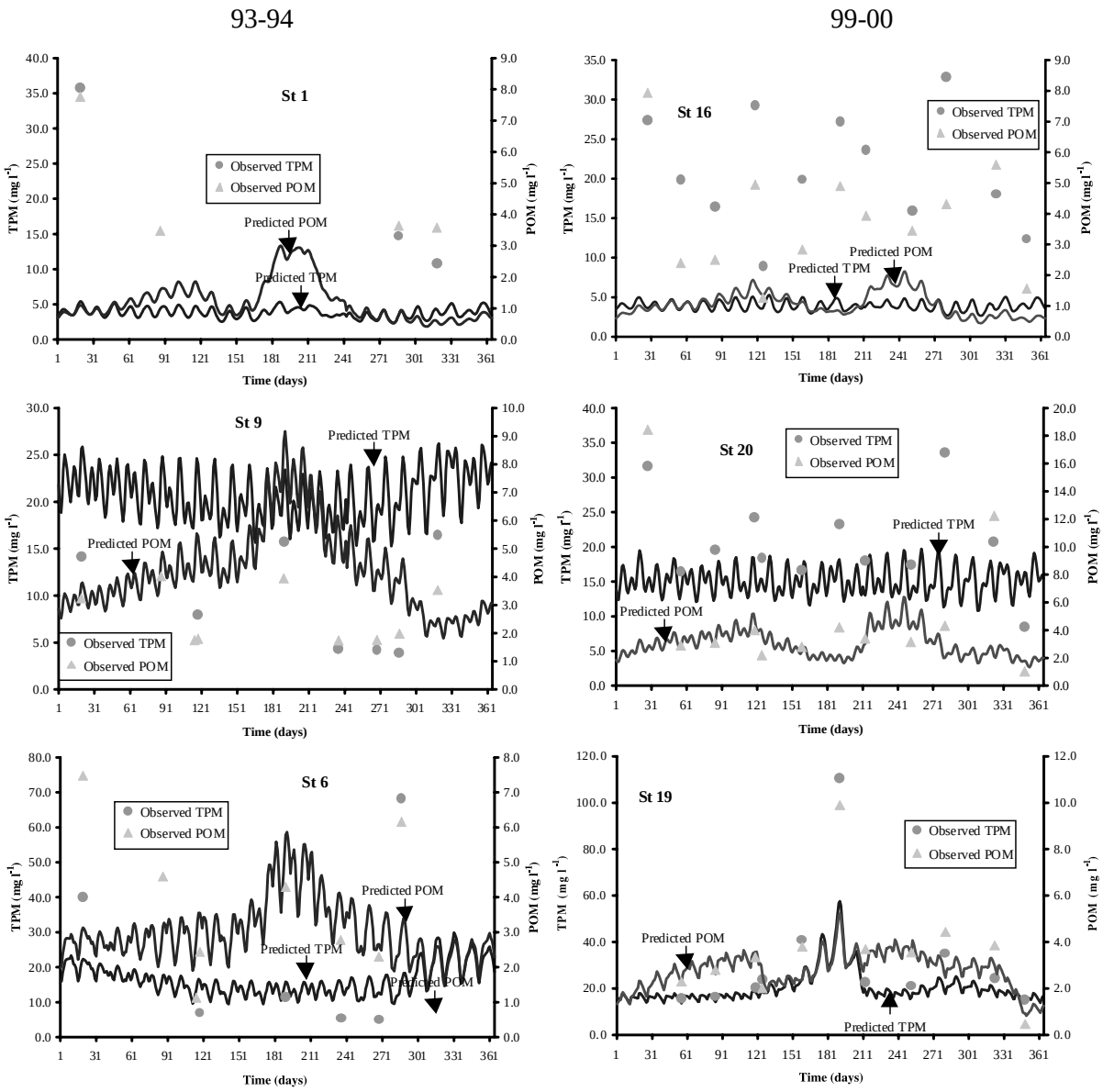

Fig. 13. Observed and predicted TPM and POM concentrations at some of the stations depicted in Fig. 4, for the scenarios I and IIa (cf. Table 6). Left charts correspond to scenario I and right charts to scenario IIa. From top to bottom, results correspond to stations at decreasing distances from the sea.

Comparing observations and predictions for scenario IIa, the model underestimated TPM at station 16 (Fig. 13). Station 16 was that closest to the inner shore of the bay. There is reasonable agreement between predicted and measured concentrations of TPM at the other sampling stations. Model predictions and observations were also in reasonable agreement for POM, except for the innermost station (Fig. 13). The slope of the Model II regression between measured and observed TPM values was S.D. from 0, whereas

Table 7
Harvest (10^3 tons DW for the kelps and FW for the bivalves) predicted under the 1993–1994 and the 1999–2000 aquaculture scenarios

Aquaculture scenarios		Kelps		Scallops		Oysters	
		Expected value	Predicted	Expected range	Predicted	Expected range	Predicted
I	93-94	40	40	43–60	55	13–24	21
IIa	99-00	28	25	10–19	9	34–46	42
IIb	99-00 (1/2)×	–	25	–	8	–	26
IIc	99-00 2×	–	25	–	0.6	–	58
IId	99-00 3×	–	25	–	0.9	–	25
IIe	99-00 1× scallops, 2× oysters	–	25	–	1.8	–	76
III	99-00 mixed scallop–kelp culture	–	25	–	33	–	42

For the latter, results are given for decreased (1/2), normal and increased (two- and three-fold) bivalve densities, including for a new scenario with mixed scallop–kelp culture. Expected ranges are given when available (cf. Sections 2 and 2.3, Table 1 and Fig. 3).

the *y*-intercept was not S.D. from 0 ($P < 0.05$). The variance explained by the model was significant ($P < 0.0001$). However, the slope was significantly higher than 1 ($P > 0.05$). These results imply that the model explains a significant proportion of the observed variance, but the differences between model and observations are proportional to the TPM concentration (Mesplé et al., 1996). Regarding POM, similar results were obtained but only after excluding station 16 results from the calculations.

3.1.7. Bivalves and kelps

Data describing scallop growth were used to calibrate an ecophysiological model with time series of measured chlorophyll, TPM, POM and temperature (Hawkins et al., 2002). A lack of data prevented similar calibration for oysters cultured in Sango Bay. Instead, parameters reported by Barillé et al. (1997) were used.

Simulated harvest yields of kelp, scallop and oyster are summarised for scenario I in Table 7. Predictions are within the estimated ranges for each species.

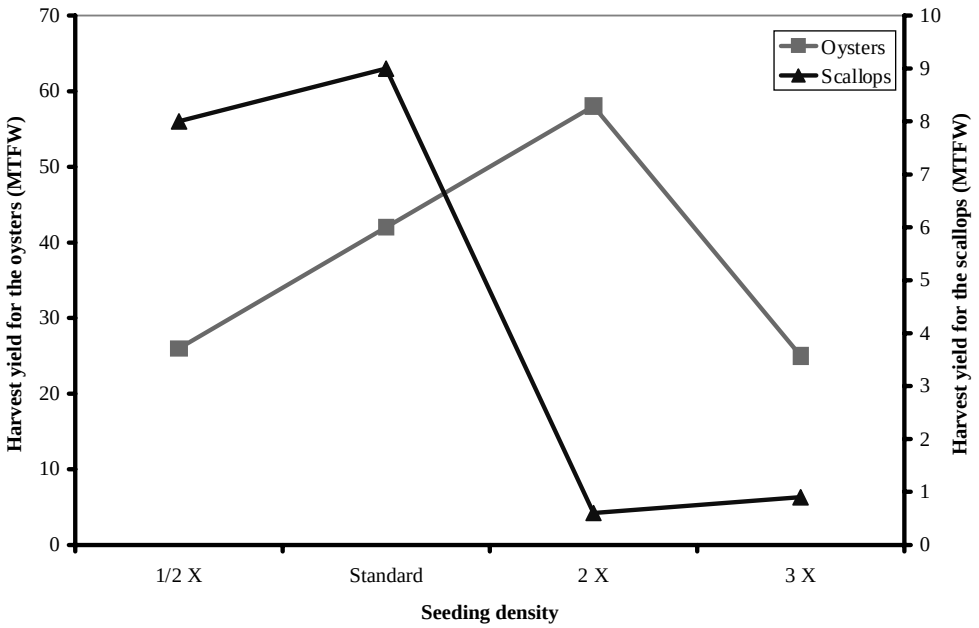

Fig. 14. 1999–2000 scenario: harvest yields as a function of seed density (refer Section 2).

The lower limits of these ranges are based on official estimates, whereas upper limits are based on known densities, including the size of each harvested species and available mortality data. Both of these limits may be subject to large errors.

Simulated harvest yields during scenario IIa are summarised in Table 7 and in Fig. 14. Model predictions are broadly within the expected ranges, albeit for scallops marginally below the lower limit of estimated harvest (Table 7). In possible explanation, the 1999–2000 prediction for scallops was obtained assuming 4.5 cm as the minimum harvest size, as they did not quite reach the official 5 cm during the normal harvest season.

Compared with scenario I, the decrease in kelp production under scenario IIa resulted from the lower initial standing stock, whereas the increase in oyster production may be explained partly by the higher initial standing stock (cf. Section 2.3). The decrease in scallop production under scenario IIa, in spite of the higher initial standing stock in scenario I (cf. Section 2.3), resulted from the shorter rearing period and harvest size.

3.2. Sungo Bay carrying capacity for bivalve culture

One of the simplest ways to assess potential effects of bivalve culture at the ecosystem scale is by comparing the time scales of water renewal, phytoplankton doubling and particle clearance by bivalves, thereby estimating the time it takes for a particular standing stock of bivalves to filter all water within the system (Dame and Prins, 1998).

Water residence time in Sungo Bay was estimated by initialising the model domain with zero salinities, assuming 35‰ salinity at the sea boundaries and running the model until salinity reached 35‰ over the whole grid. It took up to approximately 20 days before the bay was completely replaced with seawater (Fig. 15), which was well within the range estimated for other systems (Table 8). The model also predicted an average concentration of 1.5 mg m^{-3} chlorophyll throughout Sungo Bay over a year (combined average of scenarios I and IIa), and which was lower than reported for other main cultivation sites, although similar to that observed in the Ria Formosa, Portugal (1.4 mg m^{-3}), which is also a sea "dominated" system

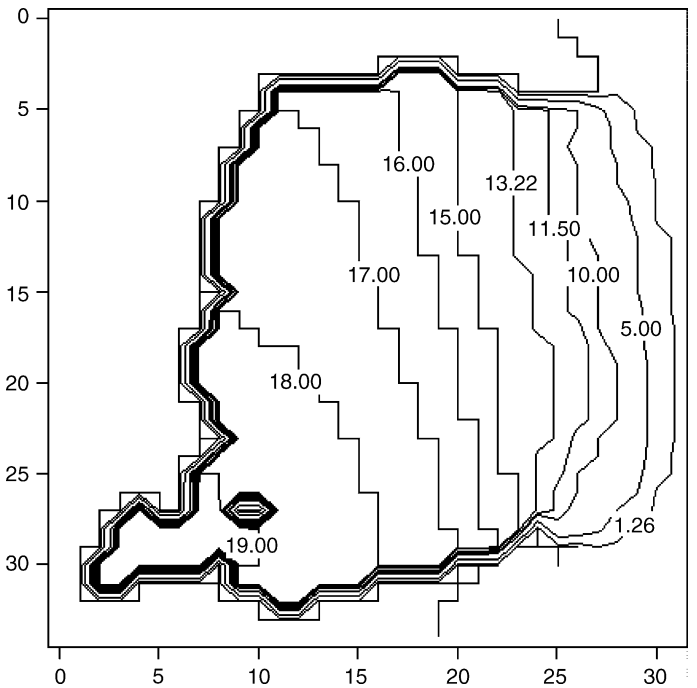

Fig. 15. Water residence times (days) at different parts of the bay, estimated from the time it takes for the sea water to replace the water inside the bay under the current culture Scenario IIa (refer text).

Table 8
Physical characteristics, phytoplankton production and bivalve grazer parameters of some coastal ecosystems (adapted from Dame and Prins, 1998 and Falcão et al., 2000) (see text)

System	Area (km^2)	Depth (m)	Volume ($\times 10^6\ m^3$)	Residence time (day)	Average annual concentration ($mg\ m^{-3}$)	Primary production ($\times 10^6$ g C per day)	Cell doubling time (day)	Total biomass ($\times 10^6$ g)	Bivalve clearance time (day)
Sylt	5.6	1.3	7	0.5	3.0	0.9	0.8	84	4.0
North Inlet	8.8	2.5	22	1.0	7.0	6.2	0.8	338	0.7
Carlingford Lough	39.5	5.0	196	65.8	3.2	1.3	16.9	14	490.2
Marennes-Oléron	135.7	5.0	675	7.1	13.0	22.2	10.0	2850	2.7
South San Francisco Bay	490.0	5.1	2500	11.1	2.6	196.0	1.1	6255	0.7
Narragansett Bay	328.0	8.3	2724	26.0	3.0	243.0	1.7	1267	25.0
Osterschelde	351.0	7.8	2740	40.0	7.5	200.0	3.1	8509	3.7
Western Wadden Sea	1386.0	2.9	4020	10.0	8.0	994.0	1.0	14700	5.8
Ria de Arosa	228.0	19.0	4335	23.0	16.0	172.7	0.6	6900	12.4
Delaware Bay	1942.0	10.0	19420	97.0	9.9	777.0	7.4	178	1278.0
Cheasapeake Bay	11500.0	7.0	27300	22.0	6.9	6006.0	0.9	1900	325.0
Ria Formosa	105.0	1.5	155	1.0	1.4	3.1	1.6	7000	4.0
Sungo Bay	179.5	10.0	1800	20.0	1.5	26.5	5.0	44000	10.1

(Table 8). Despite low chlorophyll concentrations, average total primary production of 26.5×10^6 g C per day and the average cell doubling time of 5 days were higher and faster, respectively, than for some of the other ecosystems (Table 8). This was in part due to the relative transparency of water, with an average light extinction coefficient of $0.5\,m^{-1}$ (Gazeau and Bacher, unpublished).

The total biomass of bivalve shellfish in Sungo Bay was estimated from known yields. Bivalve clearance time was calculated assuming that the average clearance rate for a commercial sized scallop of between 5 and 6 cm shell length was $2.5\,l\,h^{-1}$ (Hawkins et al., 2002), and that the average clearance rate of a commercial sized oyster of 7 cm shell length was $4\,l\,h^{-1}$ (Barillé et al., 1997). Average clearance rates were multiplied by the number of individuals at marketable size, that were 1.2×10^9 scallops and 107 million oysters, calculated from total biomass figures. The resulting time estimated for suspension-feeding bivalves to filter all water within the system averaged 10.1 days, which is about half the estimated average residence time for water renewal (Table 8). Cultured bivalves therefore depend on food made available within Sungo Bay, from sources that may include benthic resuspension and/or primary production. Indeed, the estimated average cell doubling time of only 5 days confirms this (Table 8).

It might be hypothesised, given that phytoplankton doubles its biomass in approximately half the time it takes bivalves to clear all water in the bay, that Sungo Bay is being exploited below its environmental carrying capacity, and that bivalve standing stock could be increased substantially. However, as will be discussed below, this assumes that local food depletion is not important, and that carrying capacity will not be affected by the way bivalves are distributed within the bay. The problem becomes even more complex when species interactions are considered.

Simulated harvest yields during scenario II, for different bivalve seeding densities that included a range from half to three times those currently employed, are summarised and illustrated in Table 7 and in Fig. 14, respectively. The model predicts a sharp decrease in scallop production when stock density is increased above the current value, and in oyster production when stock density is more than twice the current value. Average annual chlorophyll concentrations predicted throughout Sungo Bay declined by almost 50% as stock increased by three times from the current culture practice under scenario IIa to hypothetical scenario IId, although with proportionally smaller reductions for TPM and POM (Table 9).

Table 9
Annual mean concentrations of chlorophyll, total particulate matter (TPM) and particulate organic matter (POM) predicted by the model under the 1993–1994 (I) and the 1999–2000 aquaculture simulations IIa, IIb, IIc and IId (cf. Sections 2 and 2.3, Table 6 and Fig. 3)

	1993–1994	1999–2000			
	I	IIa	IIb	IIc	IId
Chlorophyll ($\mu g\,l^{-1}$)	1.4	1.5	2.0	1.0	0.8
TPM ($mg\,l^{-1}$)	19.6	14.9	15.1	14.6	14.5
POM ($mg\,l^{-1}$)	3.5	2.4	2.6	2.1	2.0

These results suggest that Sungo Bay is already being exploited close to the environmental carrying capacity for scallop production at the present aquaculture scenario, whereas there may be some potential for increased oyster production. Any significant increase in yield must to a great extent depend upon the relative spatial distribution of cultivated species.

The effects illustrated in Fig. 14 follow the expected parabolic response (Bacher et al., 1998). For both scallops and oysters, initial increases in harvest yields are proportionately less than expected with the doubling in stock densities, indicating growth limitation at even half the current densities. Above a certain threshold, both food limitation and reduced growth rates result in a reduction in harvest yield, when cultured species may not reach their commercial size in time for normal harvest. Under such conditions, it is conceivable that total yield may be higher at larger temporal scales than were analysed here (cf. Ferreira et al., 1998). This could happen if a large number of cultured bivalves reach harvestable size in more than 1 year. However, such considerations may be compromised by uncertainties concerning age-dependent mortality. In any case, because mass mortalities of scallops occur during summer in Sungo Bay, cultivation strategy needs to be directed towards a rearing period of less than 1 year, as at present.

There is some strong empirical evidence that bivalve mortality rate in Sungo Bay is density dependent (Fang, unpublished data). The reasons for

this dependence may be related to competition for food, degradation of water quality and/or diseases. The reduction in harvest yield when stock density is increased indicates some competition for food, when organisms may be more sensitive to diseases or other stress factors. One potential improvement in our present model would be to relate mortality with stock density and/or food limitation. The results of a sensitivity analysis to investigate the effects of changing bivalve mortality by ±10% suggest that, within this range, mortality has a low effect on final yields. For scenario IIa, a 10% increase did not produce significant changes in predicted yields (the order of magnitude of these changes was of some tens of tons). A 10% decrease produced a positive change in oyster yield, from 42×10^3 to 43×10^3 tons FW, and a negative change in scallop yield, from 9×10^3 to 8×10^3 tons FW. These changes are consistent with those reported above, under different scenarios of decreasing and increasing bivalve stocks, including the conclusion that scallops are being exploited close to environmental carrying capacity. The slight increase in predicted yield of scallops following an increase in simulated mortality stemmed from the resulting reduction in intraspecific competition for food.

Growth isolines predicted by the model under scenario I are shown for scallops and oysters in Fig. 16. Findings predict that in some areas of Sungo Bay, scallops may grow to a maximum of 7 cm shell length prior to the first harvest period during October. This is consistent with natural and predicted growth as discussed by Hawkins et al. (2002). Simulated growth curves for scenario I are illustrated in Fig. 17, showing that scallops at the site of fastest annual growth stopped growing at around Julian day 266 during October. This cessation in growth was primarily due to the effects of increasingly cold water on feeding rate (Hawkins et al., 2002). Similar behaviour was predicted for the oysters. Again, the reason was temperature limitation of feeding rate, following the responses described in Barillé et al. (1997), and which agrees with general observations by farmers that oysters in Sungo Bay may grow from around 2 mm in April to 7 cm by the time of the first harvest in November. Comparable growth has been observed in other ecosystems. In both the Bay of Marennes-Oleron (France) and Carlingford Lough (Republic of Ireland), growth from winter to autumn, before slowing to virtually zero until spring, was such that oysters achieved 12 kJ, equivalent to about 0.65 g dry soft tissue and 7 cm shell length (Raillard et al., 1993; Barillé et al., 1997; Ferreira et al., 1998).

Predicted scallop growth was lowest at the southern and north-eastern parts of Sungo Bay, and highest in the central-eastern areas. Predicted growth for oysters increased from the south-west to the north-east (Fig. 16). These trends were largely associated with higher average food availability. In contrast, predicted growth in kelp biomass was very similar throughout Sungo Bay, with biomass density reaching values close to 300 g DW m^{-2} over the whole cultivation areas, prior to harvest. These predictions could not be validated numerically, for to the best of our knowledge, there is no data available describing the natural growth of kelp during culture in different parts of the bay.

Growth isolines predicted by the model for scenario IIa are shown for scallops and oysters in Fig. 18. Findings indicate less spatial variation than under scenario I. This may reflect the smaller spatial dispersion of culture. In addition, compared with scenario I, predicted growth of scallops was considerably reduced. This is consistent with the official reduction in harvestable size from 6 cm in 1993–1994 to 5 cm shell length in 1999–2000. Slower growth may be explained by reduced food availability measured as POM, which averaged 3.5 mg l^{-1} in 1993–1994 compared with 2.4 mg l^{-1} during 1999–2000 (Table 9). Simulated growth curves for scenario IIa are illustrated in Fig. 19. Whilst growth predicted for oysters was similar to that under scenario I (Fig. 17), that for scallops, which under scenario IIa were now seeded during October, was fastest from the beginning of spring according to natural growth observed during culture as described by Hawkins et al. (2002).

Kelp final biomasses are about 5–10% higher (ca. 320 g DW m^{-2}) than during the previous culture practice represented by scenario I and, as before, very similar throughout the bay. These differences between scenarios do not reflect overall production as indicated by harvest yields, which were almost halved (Table 6), resulting from a reduction in the total area used to cultivate kelp (Fig. 3).

For oysters, the largest predicted effects of density occur in the south-eastern part of their cultivation area, with size prior to harvest being reduced by more than 20% under the higher stock density. For scallops, the

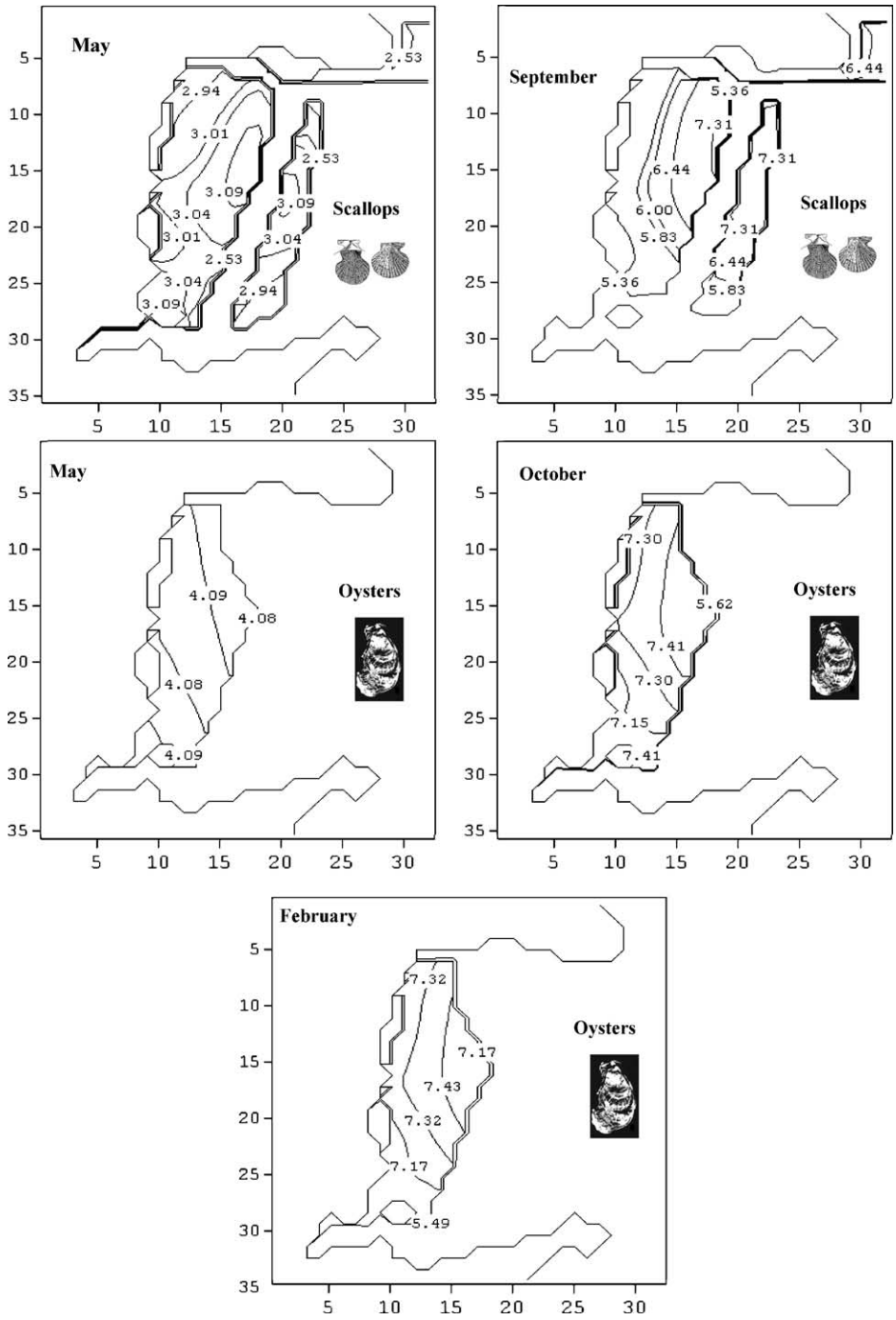

Fig. 16. Scenario I. Growth isolines (cm shell length) predicted by the model for scallops and oysters. For the former, results are shown for May, just after seeding, and for September, just before the first harvest period (top two figures). For the latter, results are shown for May, just after seeding, including for October and February, just before the first and second harvest periods, respectively (refer text).

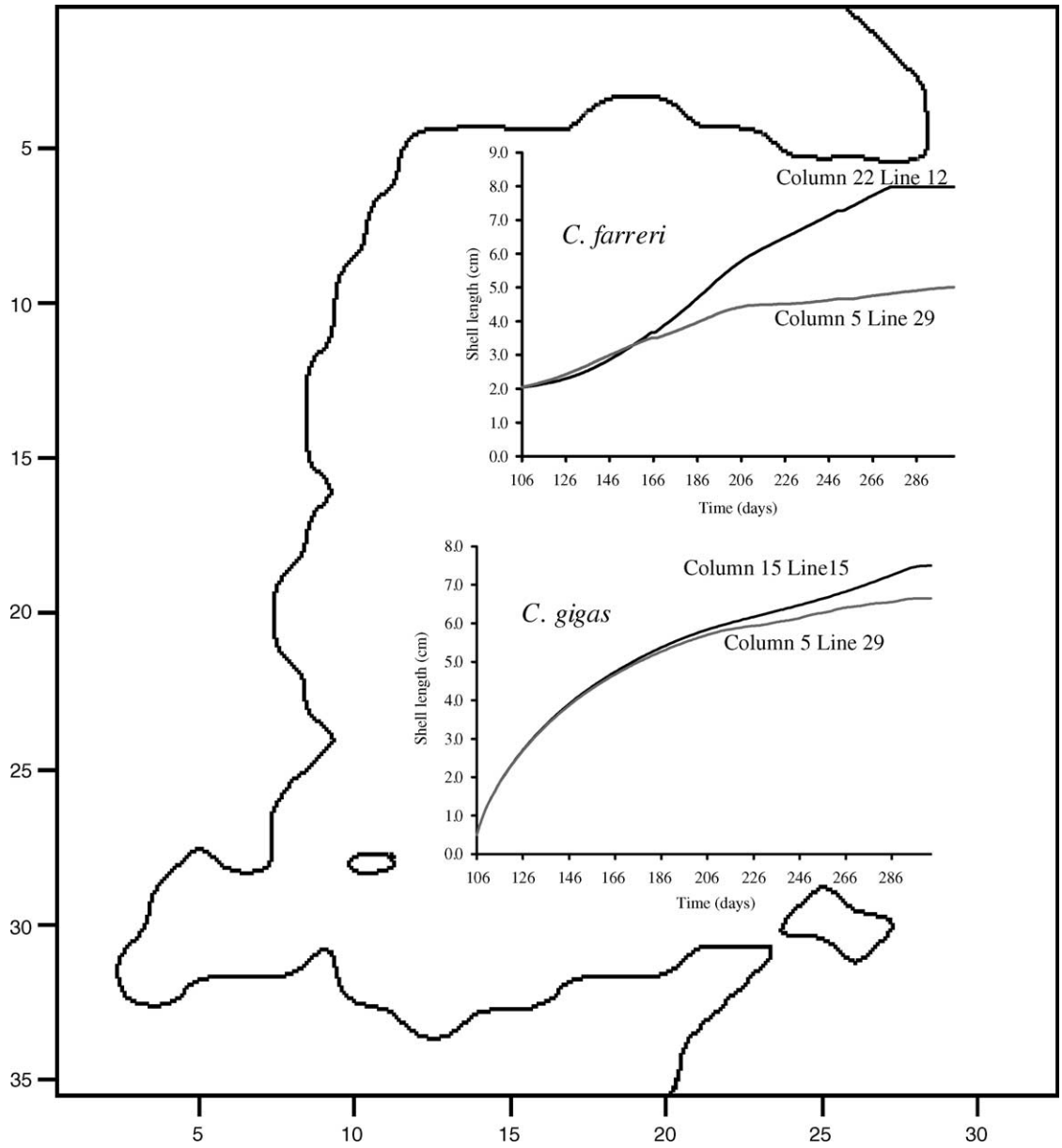

Fig. 17. Scenario I. Shell length as a function of time (Julian days) from March to November in oysters and from October to July in scallops. Also shown are coordinates of the model grid where each growth curve was calculated.

largest changes occur at the most western and southern of their cultivation areas, with size prior to harvest being reduced by more than 18% under the higher stock density. For both species, these differential spatial sensitivities may be explained, at least in part, by associated differences in water residence time, that increased from less than 5 days at the sea boundary to about 20 days in the south western corner of the bay (Fig. 15).

Because scallops appear more sensitive than oysters to stock density under current culture conditions, a hypothetical simulation was carried out with normal

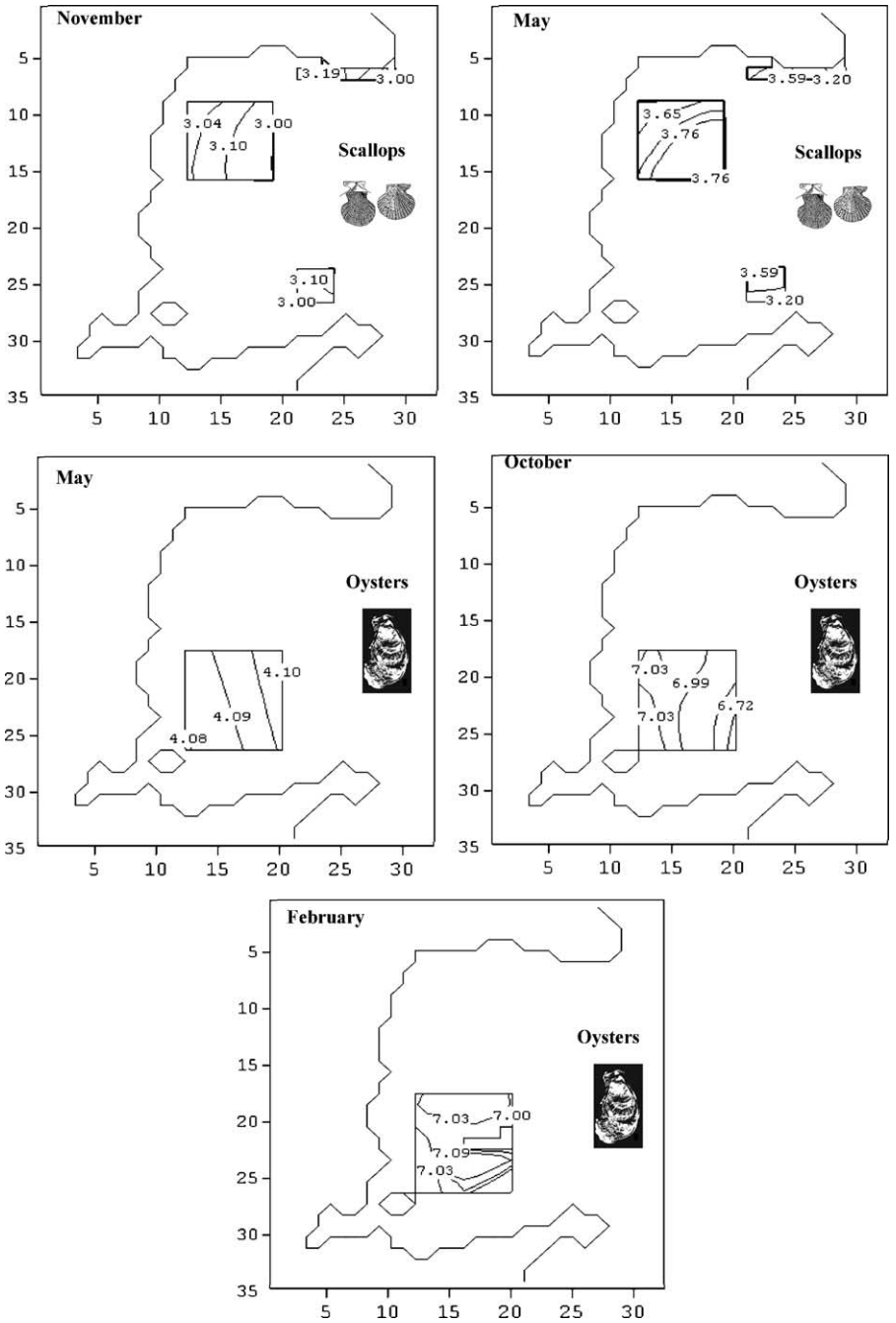

Fig. 18. Scenario IIa: growth isolines (cm shell length) predicted by the model for scallops and for oysters. For the former, results are shown for November, just after seeding, and for May, just before harvest (top two figures). For the latter, results are shown for May, just after seeding, including for October and February, just before the first and second harvest periods, respectively (refer text).

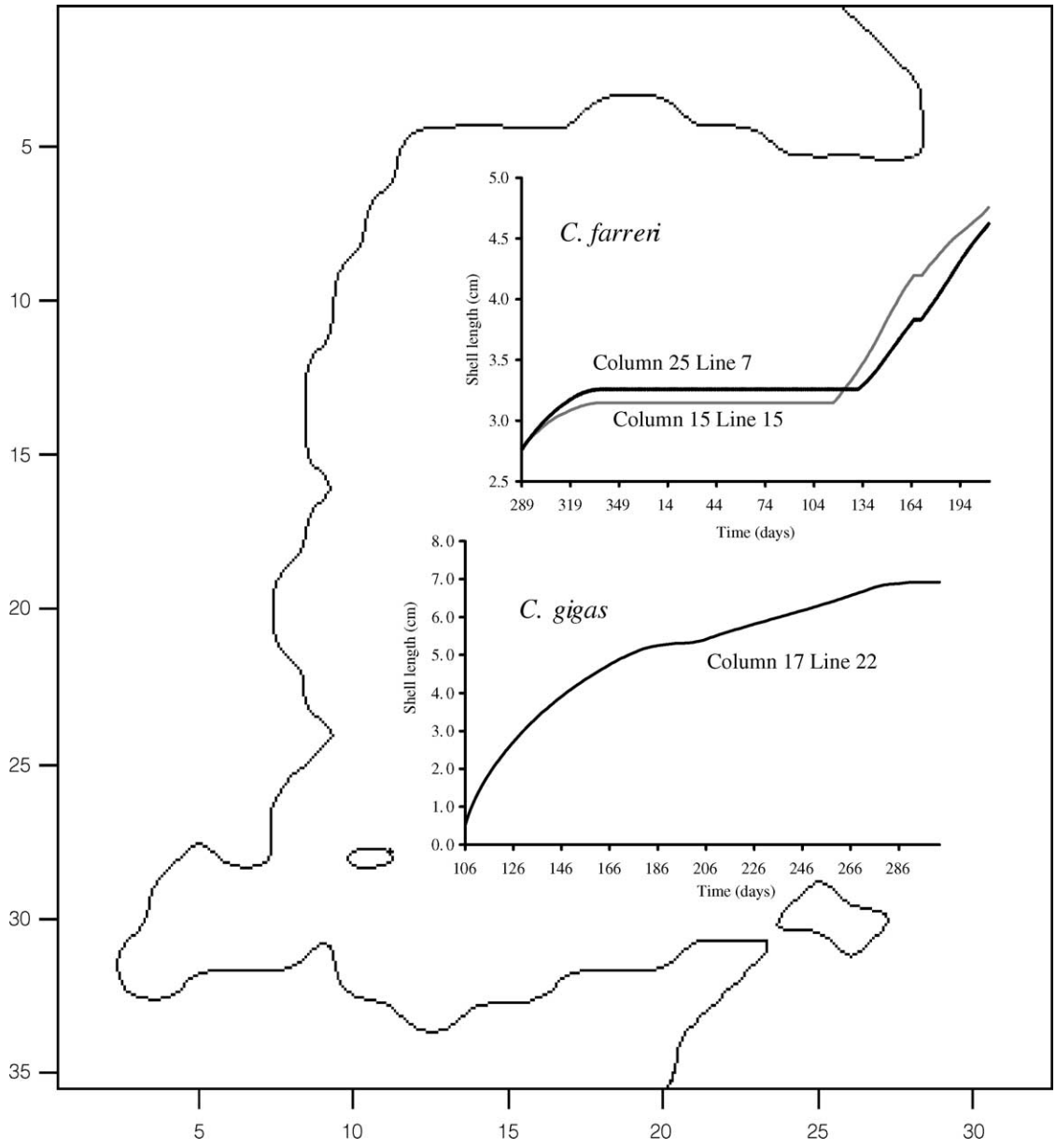

Fig. 19. Scenario IIa: shell length as a function of time (Julian days) from March to November in oysters and from October to July in scallops. Also shown, are coordinates of the model grid where each growth curve was calculated.

scallop density as under current culture practice, but with doubled oyster densities (scenario IIe). Predicted harvest yield for scallops was reduced to 1.8×10^3 tons fresh weight, compared with 9×10^3 tons under current culture practice (Table 7). In contrast, predicted harvest yield for oysters increased from 42×10^3 to 76×10^3 tons (Table 7). This suggests both intra- and interspecific competition for food, with a competitive advantage for oysters compared with scallops, despite being cultivated in different areas of the bay. Equally important, local farms may produce effects at the bay scale.

3.3. Alternative management strategy

Harvest yields predicted under scenario III indicate that oyster yield would be maintained, yet scallop production increased by more than three-fold from 9×10^3 to 33×10^3 tons by spreading and combining the same total load of scallops over a larger area that included the former cultivation areas for both scallops and kelp. This represents an increase of 47% in the total combined yield of shellfish in comparison with current aquaculture scenario (IIa) (Table 7). Interestingly, similar combinations of scallop and kelp culture have proven successful elsewhere (Scoggan et al., 1989; Ruying and Qingyin, 1992; Fang et al., 1996). Higher predicted yields not only resulted from the consequent reduction in average scallop density from 59 to 19 indiv. m^{-2}, but also because a large part of the scallop stock was moved eastwards, where water residence times are smaller (Fig. 15).

4. Conclusions

Reasonable model calibration and validation were achieved, with simulations that enable conclusions on the environmental carrying capacity for shellfish culture in Sungo Bay. Findings indicate that the ecosystem is being exploited close to its carrying capacity. Nevertheless, our model predictions also suggest that bivalve production within Sungo Bay as a whole may be increased substantially by simple alteration in the densities and/or distribution of cultured species. Given current aquaculture practice in terms of distribution and timing, varying densities alone, scallop production may not be increased over 10,000 tons (FW), whereas oyster production may not be increased over 46,000 tons (FW). However, the combined production of both oysters and scallops is higher upon increasing densities of cultured oysters, albeit at the expense of scallop production. This indicates a competitive advantage for oysters, suggesting that the culture of scallops and oysters might best be separated to avoid interspecific competition for food. Indeed, the highest total combined yield for shellfish was predicted by reducing local densities of scallops through combined culture with kelp.

Combined findings also make clear how estimates of carrying capacity may depend on the spatial scale being analysed. Density-dependent effects predicted here indicate how local farms may produce effects at the bay scale. When using a whole system approach, comparing the average temporal scales of water renewal, primary production and water filtration by bivalves, then variations in spatial distributions and densities are ignored. This may mask areas of relative food limitation, leading to possible overestimation of the total environmental carrying capacity. Where spatial variation is significant, it may therefore be important to resolve distributions and densities of each cultured species, so that any local food limitation, including that which may result from competitive interrelations between species, can be taken into account.

One of the major disadvantages of this 2D carrying capacity modelling is the computing time, which is 4 days for a simulation of 1.5 years with a 1.4 GHz processor. This makes it challenging to analyse scenarios at larger temporal scales. In addition, such a model is difficult to calibrate and validate. On the other hand, non-spatially resolved models may mask local food depletion, and tend to overestimate carrying capacity. The ideal would be to have several models with variable spatial resolution, and be able to compare and intercalibrate them in such a way that the effects of scale could be parameterised to correct the estimates of larger scale models and compensate for the density "averaging" effect described above. If this was achieved, then it would be possible to use simpler and quicker models to analyse general scenarios or larger temporal scales.

The main innovative aspects of the model presented in this work are the coupling between hydrodynamics and biogeochemistry, within the same spatial and temporal framework, and the simulation of a multi-species culture in a carrying capacity model. The main innovative findings are the dependence of carrying capacity estimates on the spatial resolution with which the ecosystem is analysed, including the dependence of carrying capacity on the spatial arrangement of cultures.

Acknowledgements

This work was supported by the INCO-DC project "Carrying capacity and impact of aquaculture on the environment in Chinese bays", contract number

ERBIC18CT980291, EU. The authors also wish to thank Professor Ramiro Neves at IST (Portugal) for his helpful comments on hydrodynamic modelling.

References

Andersen, V., Nival, P., 1989. Modelling of phytoplankton population dynamics in an enclosed water column. J. Mar. Biol. Assoc. U.K. 69, 625–646.

Bacher, C., 1989. Capacité trophique du bassin de Marennes-Oléron: couplage d'un modèle de transport particulaire et d'un modèle de croissance de l'huître *Crassostrea gigas*. Aquat. Living Resour. 2, 199–214.

Bacher, C., Duarte, P., Ferreira, J.G., Héral, M., Raillard, O., 1998. Assessment and comparison of the Marennes-Oléron Bay (France) and Carlingford Lough (Ireland) carrying capacity with ecosystem models. Aquat. Ecol. 31, 379–394.

Baretta, J., Ruardij, P. (Eds.), 1988. Tidal Flat Estuaries. Simulation and Analysis of the Ems Estuary: Ecological Studies, vol. 71. Springer-Verlag, New York, 353 pp.

Barillé, L., Héral, M., Barillé-Boyer, A., 1997. Modélisation de l'ecophysiologie de l'huître *Crassostrea gigas* dans un environment estuarien. Aquat. Living Resour. 10, 31–48.

Brock, T.D., 1981. Calculating solar radiation for ecological studies. Ecol. Model. 14, 1–9.

Carver, C.E.A., Mallet, A.L., 1990. Estimating carrying capacity of a coastal inlet for mussel culture. Aquaculture 88, 39–53.

Dame, R.F., Prins, T.C., 1998. Bivalve carrying capacity in coastal ecosystems. Aquat. Ecol. 31, 409–421.

Dike, P.P.G., 2001. Coastal and Shelf Sea Modelling. Kluwer Academic Publishers, Dordrecht.

Dowd, M., 1997. On predicting the growth of cultured bivalves. Ecol. Model. 104, 113–131.

Eppley, R.W., 1972. Temperature and phytoplankton growth in the sea. Fish. Bull. 70, 1063–1085.

Falcão, M., Duarte, P., Matias, D., Joaquim, S., Fontes, T., Meneses, R., 2000. Relatório final do projecto Gestão do cultivo de bivalves na Ria Formosa com recurso à modelação matemática. Instituto para a Conservação da Natureza, 107 pp.

Fang, J., Sun, H., Yan, J., Kuang, S., Feng, L., Newkirk, G.F., Grant, J., 1996. Polyculture of scallop *Chlamys farreri* and kelp *Laminaria japonica* in Sungo Bay. Chin. J. Oceanol. Limnol. 14, 322–329.

Ferreira, J.G., 1995. ECOWIN—an object-oriented ecological model for aquatic ecosystems. Ecol. Model. 79, 21–34.

Ferreira, J.G., Duarte, P., Ball, B., 1998. Trophic capacity of Carlingford Lough for oyster culture—analysis by ecological modelling. Aquat. Ecol. 31, 361–378.

Gazeau, F., 2000. An ecosystem model applied to an aquaculture site: Sungou Bay (China). Thesis for the D.E.A. in Modelling of the Marine Environment, Universidade Nova de Lisboa.

Gazeau, F., Bacher, C., unpublished. Assessment of the temporal and spatial variability in Sungo Bay.

Grant, J., Bacher, C., 2001. A numerical model of flow modification induced by suspended aquaculture in a Chinese Bay. Can. J. Fish. Aquat. Sci. 58, 1–9.

Guo, X., Ford, S., Zhang, F., 1999. Molluscan aquaculture in China. J. Shellfish Res. 18, 19–32.

Hawkins, A.J.S., Fang, J.G., Pascoe, P.L., Zhang, J.H., Zhang, X.L., Zhu, M.Y., 2001. Modelling short-term responsive adjustments in particle clearance rate among bivalve suspension-feeders: separate unimodal models of seston volume and composition in the scallop *Chlamys farreri*. J. Exp. Mar. Biol. Ecol. 261, 61–73.

Hawkins, A.J.S., Duarte, P., Fang, J.G., Pascoe, P.L., Zhang, J.H., Zhang, X.L., Zhu, M.Y., 2002. A functional model of responsive suspension-feeding and growth in bivalve shellfish, configured and validated for the scallop *Chlamys farreri* during culture in China. J. Exp. Mar. Biol. Ecol. 281, 13–40.

Herman, M.J., 1993. A set of models to investigate the role of benthic suspension feeders in estuarine ecosystems. In: Dame, R.F. (Ed.), Bivalve Filter-Feeders in Estuarine and Coastal Ecosystems. NATO ASI Series, pp. 421–454.

Jørgensen, S.E., Bendoricchio, G., 2001. Fundamentals of Ecological Modelling. Developments in Ecological Modelling, vol. 21. Elsevier, Amsterdam, 530 pp.

Jørgensen, S.E., Nielsen, S., Jørgensen, L., 1991. Handbook of Ecological Parameters and Ecotoxicology. Elsevier, Amsterdam, 1263 pp.

Knauss, J.A., 1997. Introduction to Physical Oceanography. Prentice-Hall, Englewood Cliffs, NJ, 309 pp.

Laws, E.A., Archie, J.W., 1981. Appropriate use of regression analysis in marine biology. Mar. Biol. 65, 99–118.

Mao, X., Zhu, M., Yang, X., 1993. The photosynthesis and productivity of benthic macrophytes in Sanggou Bay. Acta Ecologica Sinica 13, 25–29.

Mesplé, F., Trousselier, M., Casellas, C., Legendre, P., 1996. Evaluation of simple statistical criteria to qualify a simulation. Ecol. Model. 88, 9–18.

Neves, R.J.J., 1985. Étude expérimentale et modélisation mathématique des circulations transitoire et rédiduelle dans l'estuaire du Sado. Ph.D. thesis, Université de Liège.

Odum, H.T., 1973. An energy circuit language for ecological and social systems: its physical basis. In: Patten, B.C. (Ed.), Systems Analysis and Simulation in Ecology, vol. II. Academic Press, London, pp. 139–211.

Odum, H.T., 1983. Systems Ecology: An Introduction. Wiley, Toronto, 644 pp.

Parsons, T.R., Takahashi, M., Hargrave, B., 1984. Biological Oceanographic Processes. Pergamon Press, Oxford, 330 pp.

Petrell, R.J., Tabrizi, K.M., Harrison, P.J., Druehl, L.D., 1993. Mathematical model of *Laminaria* production near a British Columbian salmon sea cage farm. J. Appl. Phycol. 5, 1–144.

Portela, L.I., Neves, R., 1994. Modelling temperature distribution in the shallow Tejo estuary. In: Tsakiris, G., Santos, M.A. (Eds.), Advances in Water Resources Technology and Management. Balkema, Rotterdam, pp. 457–463.

Raillard, O., Ménesguen, A., 1994. An ecosystem model for the estimating the carrying capacity of a macrotidal shellfish system. Mar. Ecol. Prog. Ser. 115, 117–130.

Raillard, O., Deslous-Paoli, J.-M., Héral, M., Razet, D., 1993. Modélisation du comportment nutritionnel et de la croissance de l'huître japonaise *Crassostrea gigas*. Oceanologica Acta 16, 73–82.

Ruying, S., Qingyin, W., 1992. *Laminaria* culture in China. INFOFISH Int. 92, 40–44.

Scoggan, J., Zhimeng, Z., Feijiu, W., 1989. Integrated farming—polyculture. In: Culture of Kelp (*Laminaria japonica*) in China. UNDP/FAO Regional Seafarming Project RAS/86/024, pp. 125–137.

SHOM (Service Hydrographique et Océanographique de la Marine), 1984. Table des marées des grands ports du Monde. Service Hydrographique et Océanographique de la Marine, 188 pp.

Smaal, A., Stralen, M., Schuiling, E., 2001. The interaction between shellfish culture and ecosystem processes. Can. J. Fish. Aquat. Sci. 58, 991–1002.

Sokal, R.R., Rohlf, F.J., 1995. Biometry: the Principles and Practise of Statistics in Biological Research. Freeman, New York, 887 pp.

Steele, J.H., 1962. Environmental control of photosynthesis in the sea. Limnol. Oceanogr. 7, 137–150.

Vreugdenhil, C.B., 1989. Computational Hydraulics: an Introduction. Springer-Verlag, New York, 183 pp.

Wan, Z., 2001. Simulation of hydrodynamic processes in Jiaozhou and Sungo Bay. In: Carrying Capacity and Impact of Aquaculture on the Environment in Chinese Bays. INCO-DC, contract number ERBIC18CT980291, EU.

Zhao, J., Zhou, S., Sun, Y., Fang, J., 1996. Research on Sungo Bay aquaculture hydroenvironment. Mar. Fish. Res. 17, 68–79.